13th AIAA Aerodynamic Decelerator Systems Technology Conference

Clearwater Beach, May 1995

PRECISION AERIAL DELIVERY SEMINAR

RAM-AIR PARACHUTE DESIGN

J.Stephen Lingard

Martin-Baker Aircraft Co. Ltd.

Higher Denham

Middlesex

England

1 INTRODUCTION

Accurate delivery of a payload by parachute is a requirement in both the space and military fields.

The cost savings available from the recovery and re-use of expensive space vehicle elements provides an incentive to develop systems capable of allowing recovery to land sites [1]. Clearly, recovery to land engenders safety risks to population and property. Re-entry trajectories can only place recovered hardware at the position for initiation of the recovery system within certain tolerances. The recovery system must therefore have sufficient gliding capability and wind penetration to reach the designated landing site. It should also be able to achieve low vertical and horizontal velocity at landing to minimise the potential for damage to the payload. The only option for land recovery is a high reliability guided gliding parachute recovery system.

For accurate delivery of military payloads by conventional parachute system the aircraft must fly low and close to the target area. This exposes the aircraft to the risk of air defense weapons and small arms and may compromise the location of ground troops. If the aircraft flies at a safe altitude the drop accuracy is compromised due to imprecision of the drop point and the vagaries of the wind. A parachute with glide and a control system can compensate for inaccuracies in drop point and wind. The greater the glide angle the greater the offset that can be achieved for a given drop altitude.

Because of its high glide capability and its controllability the ram air parachute offers considerable scope for the delivery or recovery of payloads to a point by automatic control linked to a guidance system.

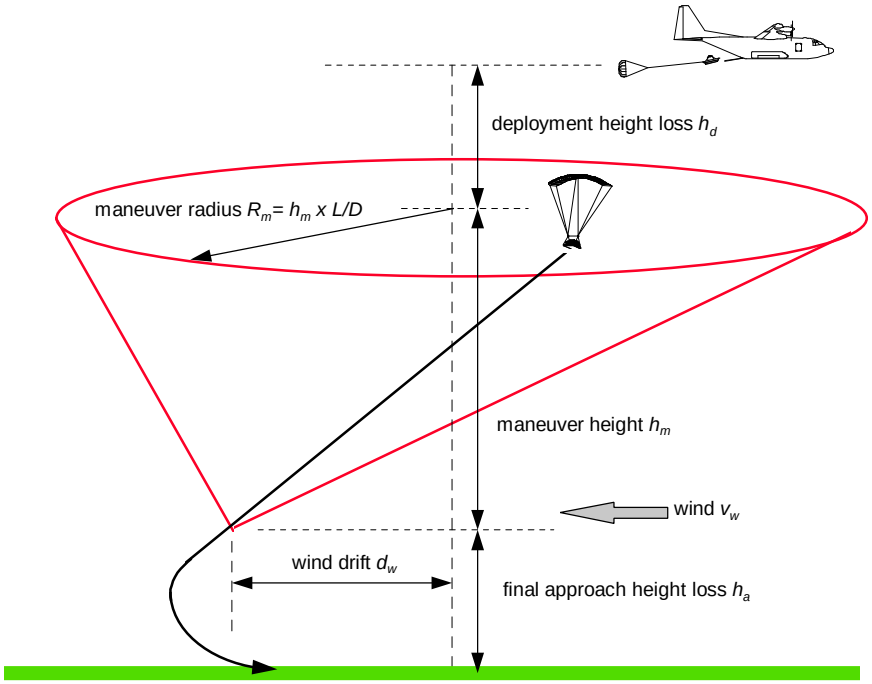

Figure 1 Precision aerial delivery mission parameters

Figure 1 shows a schematic diagram of a typical Precision Aerial Delivery System (PADS) mission. The drop is divided into three sections:

- deployment of the ram-air parachute and establishment of steady glide;
- maneuvering flight to the landing zone;
- final approach maneuver to touch down.

The altitude available for maneuver from an initial drop altitude h_0 is

$$h_m = h_0 - h_d - h_a.$$

In the absence of wind the maneuvering radius R_m from any altitude h is:

$$R_m = (h - h_a) \times L/D$$

where L/D is the parachute lift to drag ratio.

The volume within which the system can maneuver to the landing zone is therefore a cone which, in zero wind, has a half angle of $\tan^{-1}(L/D)$. Therefore, the greater the L/D of a parachute, the greater the offset of initial drop it can tolerate and the more flexible it is for the PADS role.

The effect of wind is to distort the cone. At any altitude the centre of the cone is moved by a distance $\overline{d_w}$ from the target where

$$\overline{d_w} = \int_0^h \frac{\overline{v_w}}{|w|} dh$$

where $\overline{v_w}$ is the wind vector $f(h)$

and w = rate of descent of the parachute $f(h)$.

If the parachute is placed within the distorted cone an efficient guidance system will result in accurate delivery. If the system strays outside the cone the parachute will fail to reach the target.

A typical PADS is shown in Figure 2

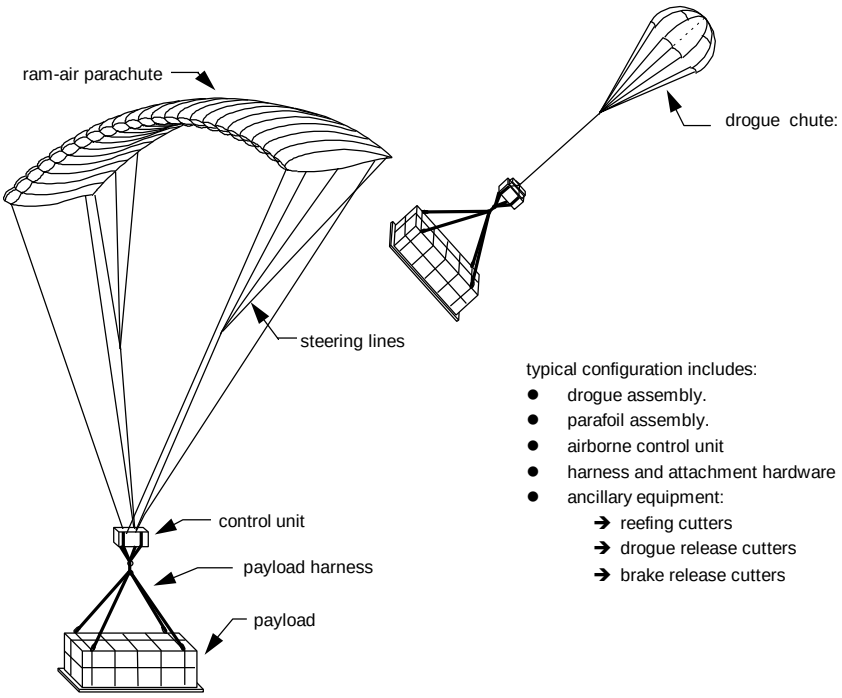

Figure 2 Precision aerial delivery system

The idea of homing gliding parachute systems is not new. The earliest systems used a directional antenna which was mounted on the airborne control system. The parachute was simply turned toward a transmitter located at the intended landing point. A refinement of his system was to introduce a dead band [2] in the control law to prevent the servo-motors from continually trying to steer the parachute. The major breakthrough in homing parachute systems was the application of GPS. This allowed the parachute to steer to a predetermined location without the need for a ground station.

The system requirements for precision aerial delivery systems are now very demanding. These are typically:

- Deployment altitude: up to 35,000 ft;
- Offset range: up to 20 km;
- Accuracy: < 100 m from planned delivery point;
- Suspended mass: 225 kg - 19,000 kg;
- Landing: soft landing desired.

The purpose of this part of the seminar is to discuss the performance and design of ram-air parachutes with particular reference to the current requirements of precision aerial delivery systems. To achieve these objectives the parachute must have:

- predictable high glide ratio;
- predictable flight speeds compatible with wind penetration;
- predictable, stable, dynamic performance in response to control inputs and wind gusts;
- predictable turn characteristics;
- reliable deployment and inflation characteristics;
- the ability to flare to reduce landing speed.

2 RAM-AIR PARACHUTE

2.1 General Description

A significant advance in parachute design occurred in the early 1960's when the airfoil or ram-air parachute (Figure 3) was invented by Jalbert.

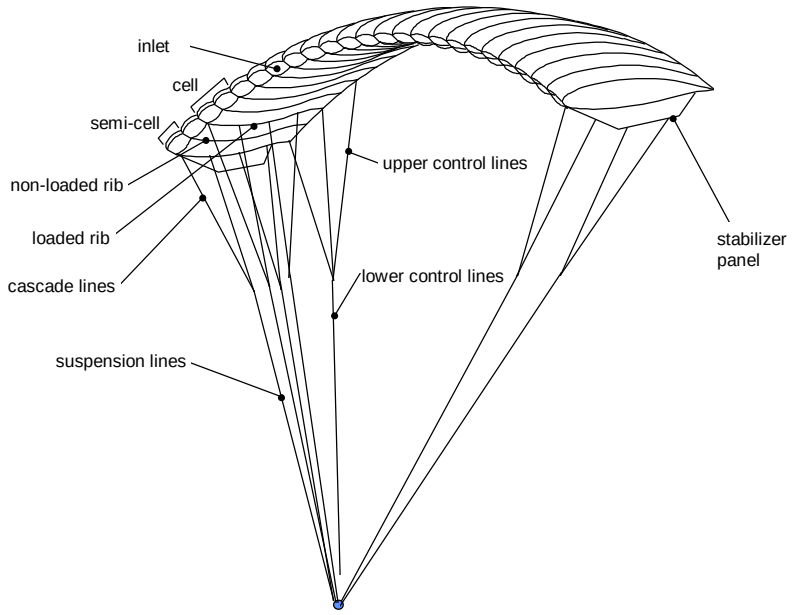

Figure 3 The ram-air parachute

The ram-air parachute, when inflated, resembles a low aspect ratio wing. It is entirely constructed from fabric with no rigid members, which allows it to be packed and deployed in a manner similar to a conventional parachute canopy. The wing has upper and lower membrane surfaces, an airfoil cross section, and a rectangular planform. The airfoil section is formed by airfoil shaped ribs sewn chordwise between the upper and lower membrane surfaces at a number of spanwise intervals forming a series of cells. The leading edge of the wing is open over its entire length so that ram air pressure maintains the wing shape. The ribs usually have apertures cut in them. This allows the transmission of pressure from cell to cell during inflation and pressure equalisation after. The fabric used in the manufacture of ram-air parachutes is as imporous as possible to obviate pressure loss.

Suspension lines are generally attached to alternate ribs at multiple chordwise positions with typically 1m spacing. Although this results in a large number of suspension lines, it is necessary in order to maintain the chordwise profile of the lower surface. Lines are often cascaded to reduce drag. Some early ram-air parachute designs have triangular fabric panels, "flares", distributed along the lower surface to which the suspension lines are attached. In addition to distributing evenly the aerodynamic load to the suspension lines and thus helping to maintain the lower surface profile, these panels partially channel the flow into a two dimensional pattern, reducing tip losses and also aid in directional stability. Whilst flares produce a truer airfoil shape with fewer distortions, improving aerodynamic efficiency, there is a penalty to be paid in weight, bulk and construction complexity. Indeed, the drag of the flares themselves possibly outweighs their advantage. Most modern designs dispense with the flares, the aerodynamic loads being distributed by tapes sewn to the ribs. Stabilizer panels are often used to provide partial end-plating and to enhance directional stability. On current designs rigging lines are typically 0.6 - 1.0 spans in length, with the wing crown rigged, that is the lines in a given spanwise bank are equal in length. The wing therefore flies with arc-anhedral.

Several airfoil sections have been used on ram air parachutes: most early wings used the Clark Y section with a section depth of typically 18% chord however recent designs have benefited from glider technology and use a range

of low speed sections (e.g. NASA LS1-0417). Various nose aperture shapes have also been investigated as nose shape affects inflation and airfoil drag. There is also a trend to reduce section depth to reduce drag but this has proceeded slowly since inflation performance can be adversely affected. Means for lateral-directional and longitudinal control are provided by steering lines attached to the trailing edge of the canopy. These lines form a crow's-foot pattern such that pulling down on one line causes the trailing edge on one side of the canopy to deflect. Turn control is effected by an asymmetric deflection of the steering lines, and angle of incidence control and flare-out are accomplished by an symmetric deflection.

The ram-air parachute has basically been refined within sports parachuting, with much of the early work experimental in nature. However, because of the perceived military and space applications and the desire to improve glide ratios, increasingly theoretical studies of ram-air performance were undertaken [3,4,5] . Reference 3 contains a comprehensive bibliography of ram-air literature up to 1980. Development of the ram-air since that time has comprised continued refinement of the basic parachute in the sports parachuting world, work to increase glide ratio [6], and development of the ram-air parachute at small scale for submunition use, up to very large scale for space applications. Puskas et al [7,8] document the development of large Paraflite canopies up to 3000 ft^2. Wailes [9] reports on Pioneer Systems / NASA work on the design of a 47 cell, 1000 lb, 11,000 ft^2 ram-air for the recovery of 60,000 lb loads. Goodrick [10] has also published a useful paper examining scaling effects on ram-air parachutes.

Chatzikonstantinou [11,12] presents a sophisticated and elegant numerical analysis to predict the behaviour of an elastic membrane ram-air wing under aerodynamic loading, solving coupled aerodynamic and structural equations. This type of analysis is essential in the extension of ram-air technology to high wing loading where the deformation of the wing is extremely significant. The equations of motion and apparent masses related to ram-air parachutes is discussed in Ref. 3 and Lissaman and Brown [13]. Brown [14] analyses turn control. The aerodynamic characteristics of ram-air wings are investigated by Gonzalez [15] who applies panel methods to determine lift curve slope and lift distribution. Ross [16] investigates the application of computational fluid dynamics (CFD) to the problem and demonstrates the potential for improved lift to drag ratio by restricting the airfoil inlet size to the range of movement of the stagnation point.

3 AERODYNAMIC CHARACTERISTICS OF RAM-AIR WINGS

3.1 General

Once inflated a ram-air parachute is essentially a low aspect wing and thus conventional wing theory is applicable. While CFD Navier Stokes and vortex panel methods can give accurate predictions of the performance of ram-air wings, a simpler approach is adopted here in order to bring out clearly the influence of the various parameters on wing performance.

3.2 Two dimensional flow around the ram-air wing section

Before embarking on the analysis of the ram-air wing, it is useful to consider the two-dimensional flow around the wing section at various angles of incidence. The flow pattern can be determined using a vortex singularity method [3]. The canopy is modelled by a vortex sheet placed to coincide with the physical location of the canopy. The strength of the sheet is determined by the application of velocity boundary conditions. The sheet strength is then used to determine the pressure distribution and circulation, and hence lift coefficient. By varying the angle of incidence, the lift curve slope dC_L/da, and the incidence angle for zero lift a_{ZL}, are found.

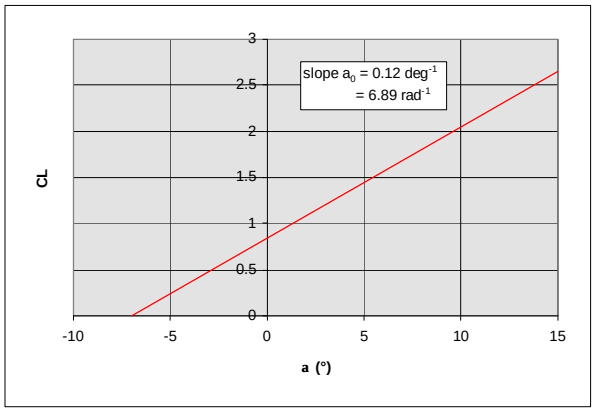

Figure 4 Theoretical section lift coefficient for an 18% Clark Y ram-air parachute airfoil

Figure 4 shows lift coefficient as a function of angle of incidence. The value of dC_L/da, a_0 = 6.89 rad^{-1} is greater than the theoretical value of $2p$ rad^{-1} for a thin airfoil, but is slightly less than the value of 7.18 rad^{-1} for an 18% thick airfoil. The zero lift angle a_{ZL} is found from Figure 4 to be -7°.

3.3 Ram-air wing lift coefficient

Although lifting line theory represents well those wings with aspect ratios above A = 5, in the case of low aspect ratio wings the trailing edge of the wing is exposed to a flow which has been deflected by the leading edge, thus the lift cannot be assumed to act on a line and must be spread over the surface of the airfoil. Also the influence of lateral edges (a minor effect for larger aspect ratios) becomes increasingly significant as aspect ratio is reduced.

Several attempts have been made to extend lifting line theory into the range of small aspect ratios, or to replace it by lifting surface theory which accounts for the effect of wing chord on lift characteristics. Lifting line theory (e.g. Pope [17]) gives the lift curve for a wing as

$$a = \frac{pa_0 A}{pA + a_0(1+t)}$$

where a_0 = the two dimensional lift curve slope

A = aspect ratio

and t is a small positive factor that increases the induced angle of incidence over that for the minimum case of elliptic loading. The parameter t is plotted for rectangular planform wings in Figure 5.

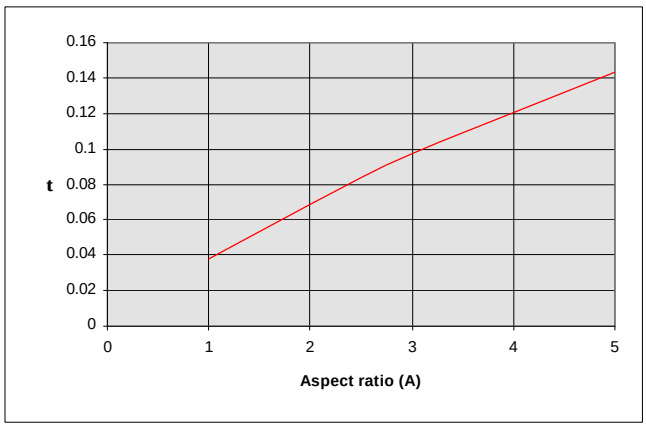

Figure 5 t for rectangular planform wings versus aspect ratio

Hoerner [18] suggests that for small aspect ratio wings the two-dimensional lift curve slope, a_0, is reduced by a factor k; that is

$$a_0' = a_0 k$$

where $$k = \frac{2pA}{a_0}\tanh\frac{a_0}{2pA}$$

and hence $$a = \frac{pAa_0'}{pA + a_0'(1+t)} \quad \text{per radian}$$

or $$a = \frac{p^2 Aa_0'}{180(pA + a_0'(1+t))} \quad \text{per degree} \qquad (1)$$

Lift curve slope derived from this function is given in Figure 6, with a_0 = 6.89 rad^{-1}.

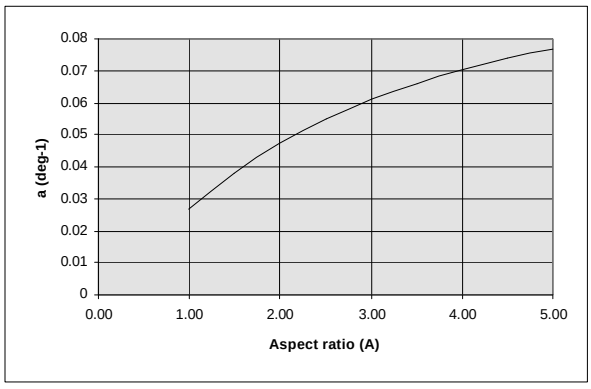

.

Figure 6 Slope of lift curve for a low aspect ratio wing versus aspect ratio

The lift curve slope of a low aspect ratio wing increases with angle of incidence over and above the basic slope determined from equation (1). The increase is a function of aspect ratio, the shape of the wing's lateral edges, and

the component of velocity normal to the wing. This non-linear component has been the subject of several investigations but is still not well understood. In some ways, however, it appears to be caused by the drag based on the normal velocity component and thus tentatively the lift increment ΔC_L may be written [18]

$$\Delta C_L = k_1 \sin^2(a - a_{ZL}) \cos(a - a_{ZL})$$

where k_1 is a function of aspect ratio and the shape of the wing's lateral edges. Reference 18 suggests that experimental data are best fitted over the range $1.0 < A < 2.5$ with

$$k_1 = 3.33 - 1.33A \qquad (2)$$

For $A > 2.5$, $k_1 = 0$

The total lift for a low aspect ratio rectangular wing before the stall may therefore be written

$$C_L = a(a - a_{ZL}) + k_1 \sin^2(a - a_{ZL}) \cos(a - a_{ZL}) \qquad (3)$$

where a is determined from equation (1) and k_1 from equation (2).

Figure 7 shows theoretical lift coefficient curves for a ram-air wing of aspect 3.0 compared with experimental data [19,20]. The zero lift angle, a_{ZL}, is taken as -7° from section 3.2 above. Up to the stall the match is acceptable. A small decrease in a_{ZL} would further enhance the fit. Below a = 0° the NASA data show a deviation from the nearly constant value of dC_L/da predicted theoretically. This appears to be caused by wing distortion and below a = 5° the NASA data are suspect. Both sets of experimental data show that ram-air canopies stall at lower angles of incidence than rigid wings of corresponding section and aspect ratio [21]. Ware and Hassell [20] and Ross [16] propose that the reason for this early stall is that the sharp leading edge of the upper lip of the open nose causes leading edge separation at relatively low lift coefficients. Conversely, Speelman *et al* [22] state that separation takes place progressively from the trailing edge. The shapes of the lift curves found by Ware and Hassell are however reminiscent of long bubble leading edge separation described by Hoerner [18]. Also, the large values of suction near the upper lip shown in Reference 3 would in practice promote leading edge separation. The NASA results show earlier stall than the Notre Dame data, stall occurring at approximately C_L = 0.7 compared with C_L = 0.85. This could be attributed to the fact that the NASA models were flexible whereas the Notre Dame models were semi-rigid. Speelman *et al* [22] emphasise the importance of maintaining a smooth, undistorted airfoil section under load, with particular attention being paid to the inlet shaping, if the aerodynamic characteristics of the wing are not to be adversely affected.

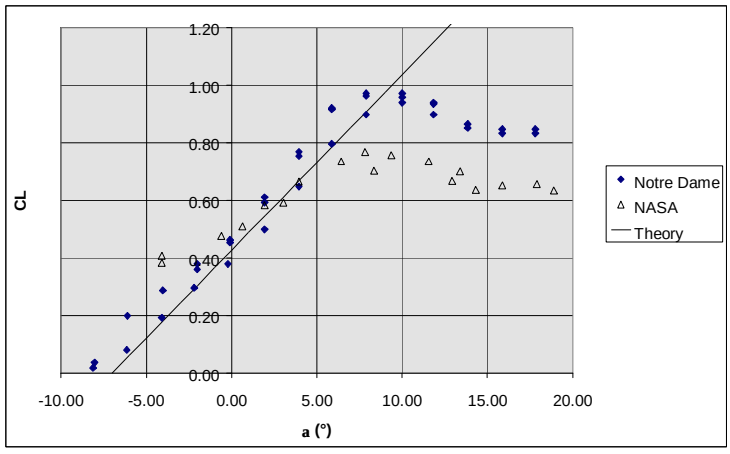

Figure 7 Experimental and theoretical lift coefficients for a ram-air wing, A = 3.0

Figure 8 shows C_L data for aspect ratios 2 to 4. It should be noted that the lift curve slope increases with increasing aspect ratio.

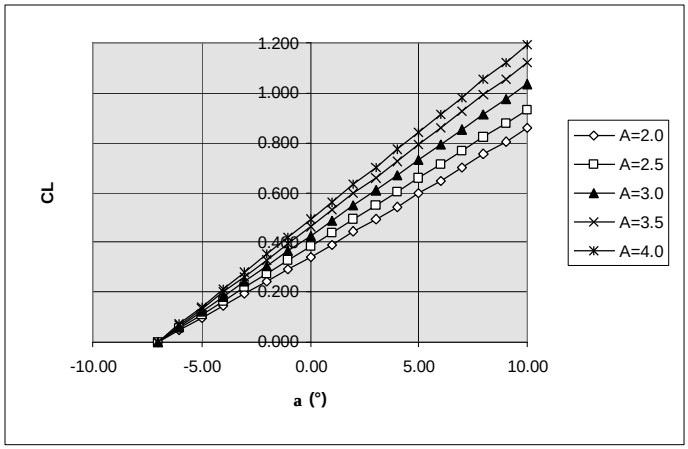

Figure 8 Theoretical lift coefficient for a ram-air wing for aspect ratios 2.0 - 4.0

3.4 Ram-air wing drag coefficient

For a rectangular wing lifting line theory gives

$$C_D = C_{D0} + \frac{C_L^{\,2}(1+\delta)}{\pi A}$$

where C_{D0} is the profile drag and the second term represents the induced drag.

The parameter δ is a small factor to allow for non-elliptic loading. Theoretical values for δ are plotted in Figure 9.

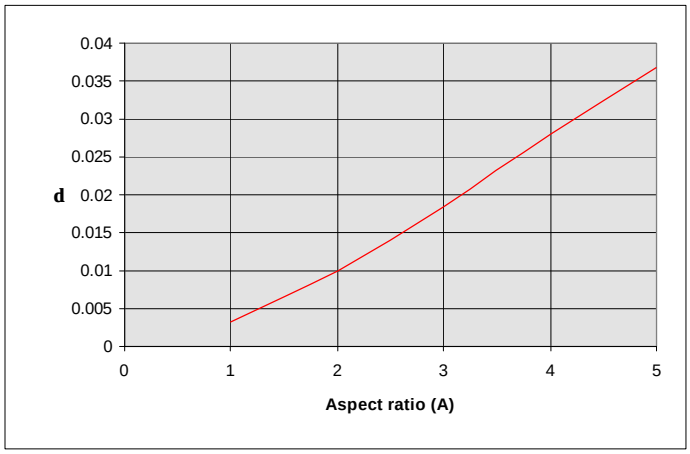

Figure 9 δ for rectangular planform wings versus aspect ratio

For small aspect ratio wings a further drag component exists, corresponding to the non-linear lift component previously described. Again assuming that this results from drag due to normal velocity, we may write [23]

$$\Delta C_D = k_1 \sin^3(\alpha - \alpha_{ZL})$$

where k_1 is identical to that for the lift component and may be found from equation (2).

The total drag coefficient for a low aspect ratio rectangular wing before the stall may thus be written:

$$C_D = C_{D0} + \frac{C_{LC}^{\ 2}(1+\delta)}{pA} + k_1 \sin^3(\alpha - \alpha_{ZL}) \qquad (4)$$

It should be noted that in this equation C_{LC} is the circulation lift coefficient $\{= a(\alpha - \alpha_{ZL})\}$ not the total lift coefficient given by equation (3), which includes the non-linear lift increment. Clearly, for a given lift coefficient the second the third terms in equation (4) decrease with increasing aspect ratio and hence, with C_{D0} remaining constant, the total drag coefficient decreases.

Ware and Hassell [20] estimate the profile drag of ram-air wings by summing the following contributory elements:

i) basic airfoil drag - for an airfoil of typical section - $C_D = 0.015$;

ii) surface irregularities and fabric roughness - $C_D = 0.004$;

iii) open airfoil nose - $C_D = 0.5\ h/c$
where h = the inlet height and c = chord length;

iv) drag of pennants and stabiliser panels - for pennants and stabilisers which do not flap this is very small (0.0001). If flapping occurs

$C_D = 0.5\ S_p / S$

where S_p is the area of pennants and stabiliser panels and S is the constructed canopy area and may be written

$S = bc$

where b = constructed wing span.

Theoretical and experimental coefficients [19,20] for a ram-air wing is presented in Figure 10 for aspect ratio 3.0. The agreement lends some credibility to the scheme of calculation proposed. Figure 11 shows drag coefficient data for a range of aspect ratios. It is interesting to note that drag coefficient at a given incidence varies little with aspect ratio.

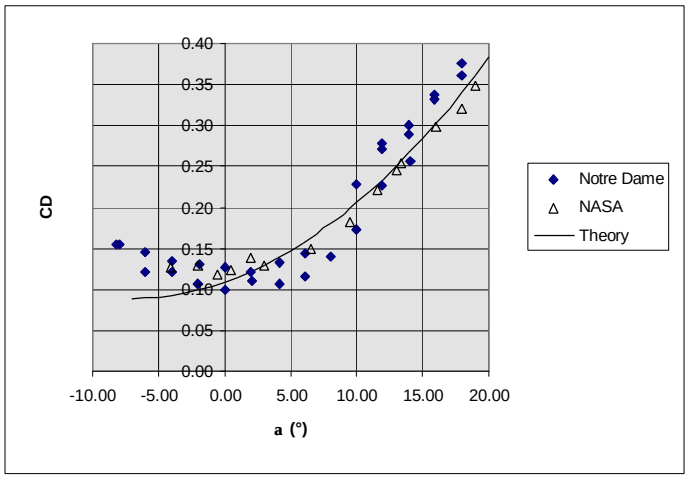

Figure 10 Experimental and theoretical drag coefficient for a ram-air wing, A = 3.0

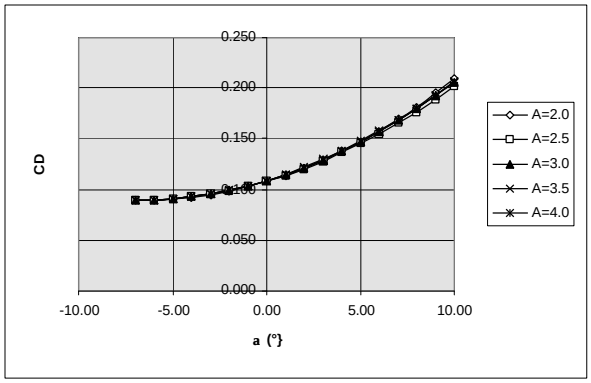

Figure 11 Theoretical drag coefficient for ram-air wings, A =2.0 - 4.0

3.5 Ram-air wing lift-drag ratio

Theoretical and experimental values of *L/D* for the wing alone are shown in Figure 12.

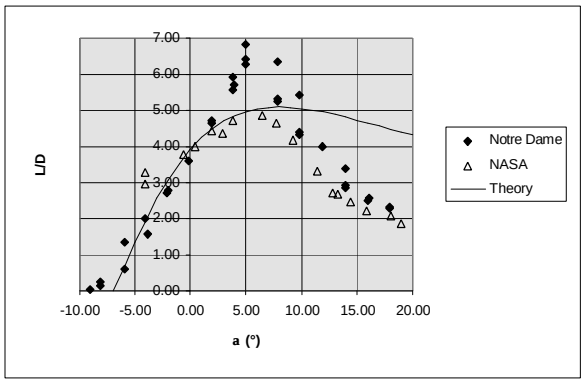

Figure 12 Experimental and theoretical L/D ratio for a ram-air wing, A = 3.0

Up to the stall the agreement with the NASA data is quite good, particularly in respect of the maximum value of *L/D* of a little over 5.0. Notice that the maximum theoretical value of *L/D* occurs close to the stall (see Figure 7).

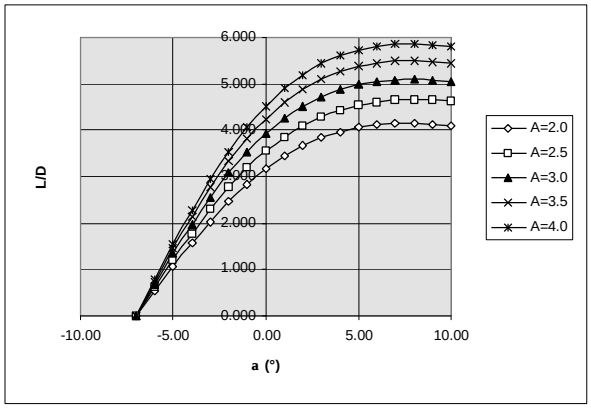

Figure 13 Theoretical L/D for ram air wings, A = 2.0 - 4.0

Figure 13 shows *L/D* ratio for a range of aspect ratios. The expected improvement of *L/D* ratio with increasing aspect ratio is shown. Theory predicts that for the wing alone maximum *L/D* increases from 4.15 at $A = 2.0$ to 5.86 at $A = 4.0$.

4 AERODYNAMIC CHARACTERISTICS OF RAM-AIR PARACHUTES

4.1 General

The incorporation of a ram-air wing into a parachute system necessitates the addition of suspension lines. Some early ram-air parachutes were rigged such that the wing flew flat. Reference 3 shows that this necessitates very long suspension lines (> 2.25 spans) to give spanwise stability of the wing. Lines of this length create substantial drag, overwhelming any gains in lift achieved. Ram-air wings are thus rigged with the lines in any chordwise bank of equal length, giving the wing arc-anhedral. This is called crown rigging. Arc-anhedral is slightly detrimental to the wings lifting properties whilst the drag coefficient for a given incidence angle remains as that for a flat wing. The suspension lines themselves add considerably to the total drag.

The amount of arc anhedral is a function of the ratio of line length (*R*) to span (*b*). From the above it is apparent that the wing alone performance improves with increasing aspect ratio but, for a given value of *R/b*, the larger the aspect ratio the greater the line length. In addition, the number of lines tends to increase with aspect ratio. Thus increasing aspect ratio gives markedly higher line drag. Reducing *R/b*, for a given aspect ratio reduces line drag but yields an increasingly inefficient wing. It is clear, therefore, that the performance of the complete parachute system is significantly different to that for the wing alone. The result of introducing arc-anhedral and line drag are therefore considered here.

4.2 Ram-air parachute lift coefficient

With the wing incorporated into ram air parachute arc-anhedral is introduced. For a conventional wing with dihedral angle defined as shown in Figure 14, Ref. 18 indicates that

$$C_L = C_{Lb=0} \cos^2 b \ .$$

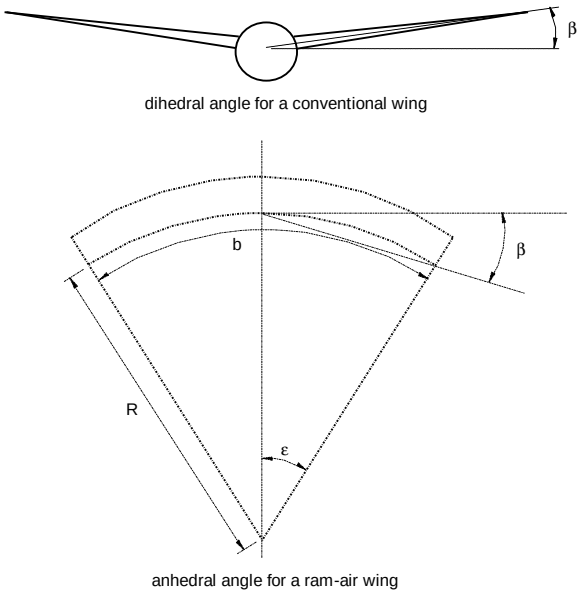

Figure 14 Definition of anhedral angle for a ram-air wing

This equation may be shown to remain valid for a wing with arc-anhedral if *b* is defined as in Figure 14. Referring to Figure 14:

$$b = e/2$$

but

$$e = b/2R$$

hence

$$b = b/4R \text{ rad or } 45b/pR°.$$

Equation (3) may now be re-written for a ram air wing with arc-anhedral:

$$C_L = a(a - a_{ZL})\cos^2 b + k_1 \sin^2(a - a_{ZL})\cos(a - a_{ZL}) \quad (5)$$

where in the absence of any information on the effect of arc-anhedral on k_1 it is assumed that k_1 remains unchanged.

The effect of line length on wing lift coefficient is shown in Figure 15.

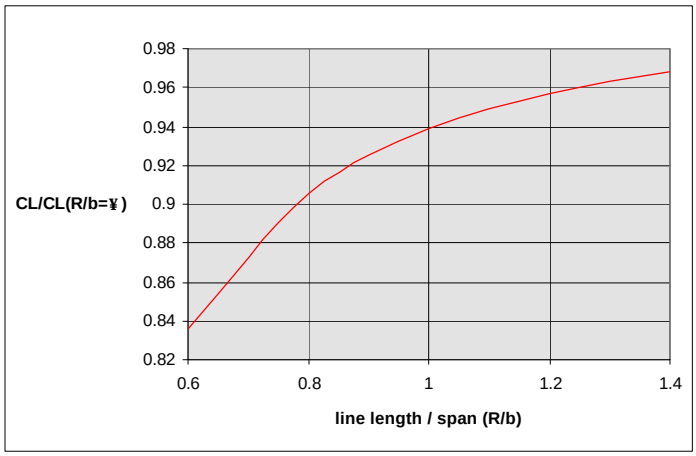

Figure 15 Influence of line length on the lift coefficient of a ram-air wing A = 3.0

4.3 Ram-air parachute drag coefficient

The overall drag of a gliding parachute system comprises the sum of wing drag, line drag and store drag; line drag and store drag contributing significantly.

To simplify the estimation of line drag it is assumed that all lines are the same length and are subject to the same normal velocity $V\cos a$ where V is the system velocity. For typical Reynolds numbers the drag coefficient of a suspension line would be approximately 1.0. The contribution of line drag to the total system drag may therefore be estimated from

$$C_{Dl} = \frac{nRd\cos^3 a}{S} \quad (6)$$

where n = the number of lines
R = mean line length
d = line diameter
and S = canopy area

Store drag coefficient may be written

$$C_{Ds} = \frac{(C_D S)_s}{S}$$

where $(C_D S)_s$ = store drag area

Induced drag and profile drag for a wing with anhedral remain approximately constant [23]; therefore the drag coefficient for a ram-air parachute system with arc-anhedral may finally be written from equation (4)

$$C_D = C_{D0} + C_{Dl} + C_{Ds} + \frac{a^2(a - a_{ZL})^2}{pA}(1+ d) + k_1 \sin^3(a - a_{ZL}) \qquad (7)$$

where A = the aspect ratio based on constructed span b.

4.4 Ram-air parachute lift-drag ratio

Typically the maximum theoretical value of lift to drag ratio occurs close to or beyond the stall for a conventional ram-air parachute. The maximum *L/D* is therefore not a useful measure to use for the performance of a ram-air parachute since, the wing cannot operate effectively close to the stall. Current ram-air parachutes are generally rigged to fly with a lift coefficient of around 0.5. To compare the performance of various configurations we will therefore consider *L/D* ratio at this practical value of C_L.

The basic parachute design considered in this section is as follows:

- aspect ratio A = 3.0
- inlet height $h = 0.14c$
- line length $R = 0.8b$
- line diameter d = 2.5 mm
- number of lines = 1 line per 12 ft^2 (= 1 line per 1.11 m^2)
- payload drag coefficient C_{Ds} = 0.006

The value of *L/D* ratio for varying aspect ratios and line lengths is shown in Figure 16, for a ram-air parachute of 300 m^2 area with 270 lines. It is clear that for large ram-air parachutes performance is considerably worse than for the wing alone. The best performance is achieved with the largest aspect ratio and the lower line length to span ratios of 0.5 - 0.6. For all aspect ratios performance decreases with increasing line length. At line length to span ratio 0.8 there is little improvement in performance with increasing aspect ratio. At large line length to span ratios the smaller aspect ratio wings yield the best performance. These trends are explained by the influence of line drag. At low values of *R/b* the reduction in induced drag with increasing aspect ratio exceeds the rise in drag due to the longer lines. At higher values of *R/b* the increasing line drag with aspect ratio overwhelms the decreases in induced drag.

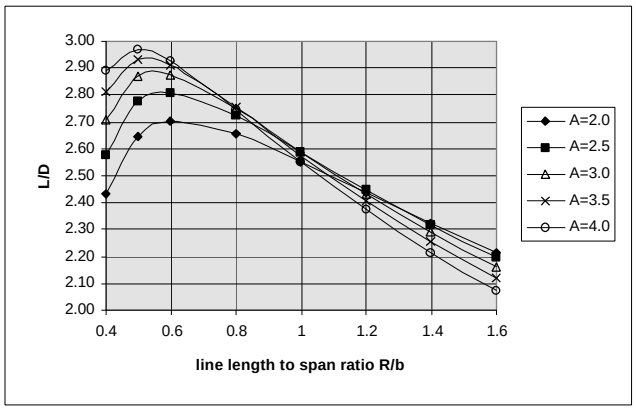

Figure 16 Theoretical L/D for a 300m^2 ram-air parachute with various aspect ratios and line length to span ratios

Figure 17 shows *L/D* ratio for varying aspect ratios and line lengths for a 36 m^2 ram air parachute with 32 lines. Different trends to those for the large canopy are apparent. Again performance is significantly poorer than for the wing alone, but not as bad as for the large ram-air. At all values of *R/b* performance increases with aspect ratio but gains become less significant at the longer line lengths. That implies that at this scale line drag is less significant. The reduction of induced drag with increasing aspect ratio is always greater than the increase in line drag. For A < 3.5 there is an optimum value of *R/b* of 0.8. Below *R/b* = 0.8 the falling wing efficiency is more significant than the decrease in line drag. Above *R/b* = 0.8 wing efficiency gains are less significant and line drag increases predominate.

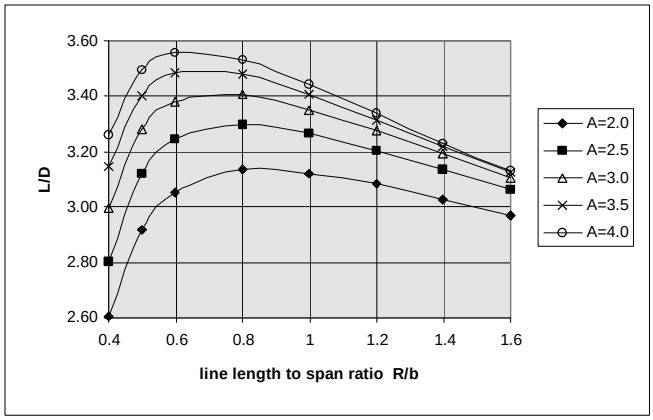

Figure 17 Theoretical L/D for a 36m^2 ram-air parachute with various aspect ratios and line length to span ratios

The difference in performance of the two sizes of ram-air parachute is of most concern for PADS. An examination of equations (6) and (7) reveals the problem. All contributions to total drag are proportional to wing area with the exception of line drag. Typically, ram air parachutes are designed with the number of suspension lines proportional to the area of the parachute. Moreover, if the canopy is scaled with constant wing loading, and a constant inflation g load is assumed, line diameter is also constant. Examining equation (6):

$$C_{Dl} = \frac{nRd\cos^3 a}{S}$$

nd/S is constant and C_{Dl} increases with line length *R*. Therefore simply scaling up a ram-air wing reduces its performance. For the basic design of *L/D* at C_L = 0.5 varies with area as shown in Figure 18.

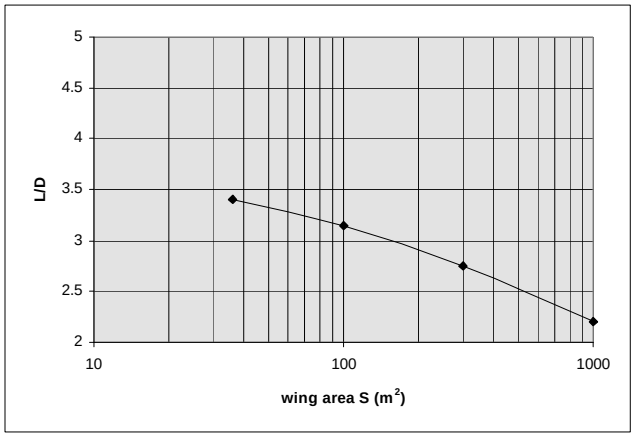

Figure 18 Lift to drag ratio versus wing area for the basic design with inlet height 0.14*c*, C_L = 0.5

For gliding parachutes to have acceptable performance at large scale it is therefore necessary to considerably improve the wing design.

4.5 Gliding parachute performance improvement

Improvements in system glide performance may be achieved by reducing system drag, which comprises the profile drag of the store, suspension lines and wing and the induced drag of the wing, or by increasing working lift coefficient (C_{Lmax}). To achieve acceptable performance it is necessary to consider both approaches. Generally effort aimed at reducing drag is, as with all airborne devices, yields most benefit.

It is useful to examine the drag contributions to a typical ram-air parachute to give an indication of where effort at drag reduction will be most effective. For a 300 m^2 ram-air parachute:

Basic airfoil drag	= 0.015 (8.2%)
Roughness drag	= 0.004 (2.2%)
Inlet drag *0.5 h/c*	= 0.070 (38.5%)
Induced drag at C_L = 0.5	= 0.033 (18.1%)
Line drag	= 0.054 (29.7%)
Store drag	= 0.006 (3.3%)
TOTAL	= 0.182

For a 36 m^2 canopy:

Basic airfoil drag	= 0.015 (10.2%)
Roughness drag	= 0.004 (2.7%)
Inlet drag *0.5 h/c*	= 0.070 (47.6%)
Induced drag at C_L = 0.5	= 0.033 (22.5%)
Line drag	= 0.019 (12.9%)
Store drag	= 0.006 (4.1%)
TOTAL	= 0.147

The significant difference between the two is the substantially larger line drag for the 300 m^2 canopy.

For the 300 m^2 canopy basic airfoil drag and roughness drag only contribute 10.4% of total drag and are clearly difficult to improve. Nonetheless, more modern wing sections, such as the LS-1 series, have lower profile drag than the Clark Y from which these data were derived, and could yield benefits. Maintenance of section by correct rigging and load distribution is essential to keep these factors low.

Store drag is not within the control of the parachute designer.

Reduction of the three remaining drag producing elements are where most gains may be made.

For large ram-air wings low values of *R/b* should be used. There is extensive practical experience at *R/b* = 0.6 and therefore this value is recommended since, although *R/b* = 0.5 is regularly used for sports parachutes, the gains in using shorter lines are not substantial and we are here at the limits of the theory. For a given line length, line drag may be decreased by reducing the number of lines provided the wing remains undistorted under load. Cascading of lines is standard practice on sports ram air parachutes and is now being used on larger ram-air parachutes. Cascading would reduce line drag by approximately 20% thus *L/D* for the large parachute would rise from 2.75 to 2.90.

Together inlet drag and induced drag contribute 56.6% of the total drag of the 300m^2 system. Clearly, before any significant improvement in ram air wing performance can be realised, one or both of these elements must be

considerably reduced. Figure 16 shows that increasing aspect ratio beyond 3.0 without other improvements is ineffective since reduced induced drag is simply traded with increased line drag. To yield significant improvements inlet drag must be reduced.

The basic 18% Clark Y airfoil has an 11% inlet height at the ribs, with 15% between ribs. This gives an average inlet height of 14%. Increasing scale will reduce the amount of bulge between ribs, since the cell width typically remains constant in scaling up the wing - due to constant line spacing - whilst the height of the cell increases. For a 36m^2 wing with unloaded ribs, the cell depth to width is typically 0.8 but for the 300m^2 parachute with only loaded ribs this becomes 1.6. Bulge will therefore be approximately halved giving a smoother wing with height typically 12.5%. Applying this correction increases *L/D* for the large wing from 2.75 to 2.86.

Once the parachute is gliding it is strictly only necessary to have an inlet height which covers the range of movement of the stagnation streamline. Ross [16] shows that a 4% inlet is feasible, however, since inflation must not be compromised reductions in inlet height should be conservative. Wings with 8.4% inlet height at the ribs are flying therefore 8% overall height is realistic. With this value performance is significantly enhanced as shown in Figure 19.

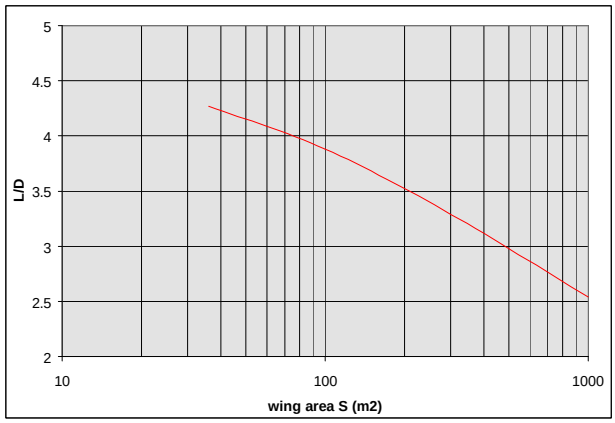

Figure 19 Lift to drag ratio versus wing area for the basic design with inlet height 0.08*c*, C_L = 0.5

An additional benefit of reduced inlet height is reduced disruption of the flow over the upper leading edge of the wing and consequently delayed stall. Ross [16] shows that for an 8.4% inlet stall does not occur until C_L = 0.85 and with a 4% inlet stall is further delayed to C_L = 1.55. It is therefore possible with reduced inlet height to increase the design lift coefficient. Figure 20 demonstrates the increased benefits of this strategy. A further improvement in performance comes out of increasing design lift coefficient in that if flight speed is maintained then wing area can be reduced giving further *L/D* gains.

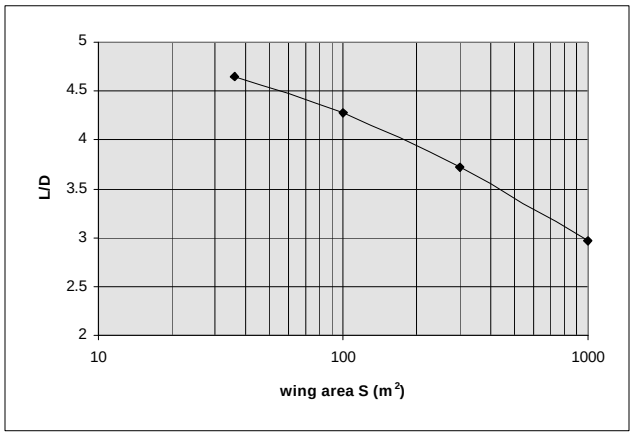

Figure 20 Lift to drag ratio versus wing area for the basic design with inlet height 0.08*c*, C_L = 0.65

Clearly for large scale ram-air parachutes detailed attention to drag reduction is essential.

⇒ Greater attention must be paid to inlet design. Inlet height should be minimised subject to maintaining inflation reliability. Vortex panel methods can be used to determine to stagnation point range.
⇒ The number of lines should be minimised subject to maintaining the airfoil shape without undue distortion.
⇒ Cascading of lines should be employed.
⇒ Line length should be optimised. R/b = 0.6 is a good design point.
⇒ Aspect ratio 3.0 is a good design point.

5 RAM-AIR PARACHUTE FLIGHT PERFORMANCE

Figure 21 shows a gliding parachute in steady descent in still air with a velocity V and gliding angle γ.

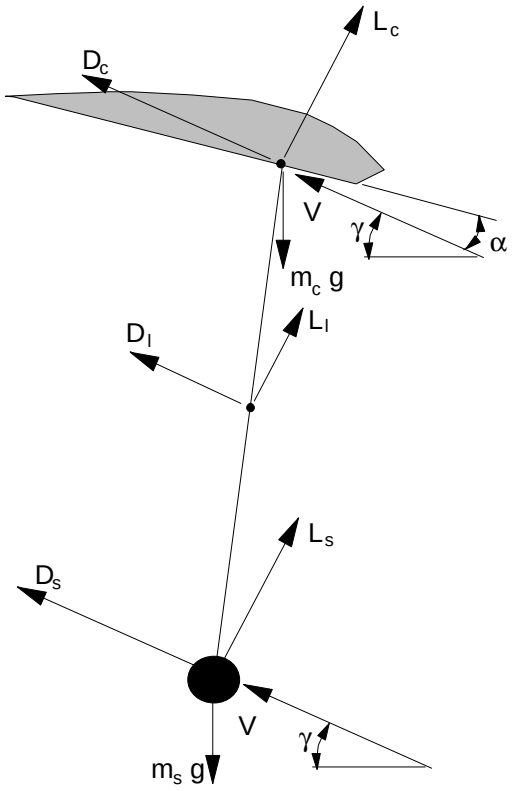

Figure 21 Ram-air parachute in steady gliding flight

Resolving the forces acting on the system horizontally and vertically:

$$\left(L_c + L_l + L_s\right)\sin g - (D_c + D_l + D_s)\cos g = 0 \tag{8}$$

$$(m_s + m_c)g - \left(L_c + L_l + L_s\right)\cos g - (D_c + D_l + D_s)\sin g = 0 \tag{9}$$

where
L_c = lift force acting on the canopy
L_l = lift force acting on the suspension lines
L_s = lift force acting on the payload
D_c = drag force acting on the canopy
D_l = drag force acting on the suspension lines
D_s = drag force acting on the payload
m_s = mass of the canopy
m_c = mass of the store
g = acceleration due to gravity

From equation (8)

$$L / D = C_L / C_D = 1/\tan g \tag{10}$$

where $L = L_c + L_l + L_s =$ total system lift

$D = (D_c + D_l + D_s) =$ total system drag

$C_L = L / 0.5\rho V^2 S =$ lift coefficient

$C_D = D / 0.5\rho V^2 S =$ drag coefficient

$S =$ reference area

$\rho =$ air density.

Equation (10) is the standard equation of aerodynamic efficiency in gliding flight. The smaller the glide angle the higher becomes the lift-drag ratio and the greater the gliding range for a given height loss.

Writing equation (9) in coefficient form and transforming:

$$W = 0.5\rho V^2 S(C_D \cos \gamma + C_L \sin \gamma)$$

where $W = (m_s + m_c)g =$ system weight.

Substituting from equation (10) and simplifying gives:

$$W = 0.5\rho V^2 S(C_L^{\ 2} + C_D^{\ 2})^{0.5} \tag{11}$$

or $$W = 0.5\rho V^2 S C_T$$

where $C_T = (C_L^{\ 2} + C_D^{\ 2})^{0.5} =$ tangent coefficient . (12)

The velocity of the parachute system in steady gliding flight may therefore be written:

$$V = \left(\frac{2}{\rho} \cdot \frac{W}{S} \cdot \frac{1}{(C_L^{\ 2} + C_D^{\ 2})^{0.5}} \right)^{0.5} . \tag{13}$$

The horizontal (u) and vertical (w) velocity components of the system may be calculated from:

$$u = V \cos \gamma$$
$$w = V \sin \gamma. \tag{14}$$

Equation 10 shows that in still air conditions glide angle, and therefore glide distance for a given height loss, is a function only of lift to drag ratio. However, equation 13 indicates that velocity V is dependent on wing loading (W/S), air density, and the aerodynamic characteristics of the parachute. Consequently, in still air conditions, a given parachute will travel the same distance for a given height loss whatever the altitude or wing loading, but velocity down the glide path will increase with increasing altitude and wing loading.

It is obvious that penetration of the wind is essential for effective PADS operation. Using a design lift coefficient of 0.5 and a range of L/D ratios typical vertical and horizontal velocities for ram-air parachutes for varying wing loading are shown in Figure 22.

For PADS systems to give some margin over possible winds, flight velocity is usually chosen to be >20m/s; that is a wing loading in the range of 15 - 20 kg/m^2 or 3 - 4 lb/ft^2.

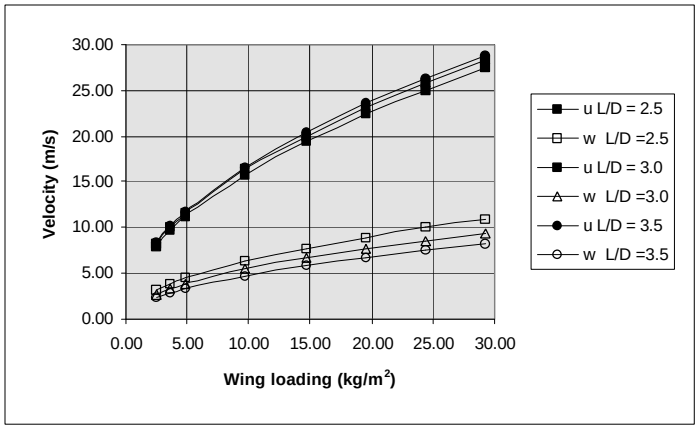

Figure 22 Ram-air parachute flight velocities versus wing loading

6 RAM-AIR PARACHUTE LONGITUDINAL STATIC STABILITY

6.1 Canopy Rigging

So far in this discussion it has been assumed that the system can be induced to fly at the angle of attack corresponding to the optimum *L/D*. The practical means of achieving this is by rigging the canopy; that is positioning the payload, and hence the CG of the system, such that the equilibrium attitude is at the required angle of attack. The parachute will be in stable equilibrium when the sum of moments acting on the system is zero and when the slope of the pitching moment curve, dC_M / da , is negative - that is when any small disturbance from equilibrium results in a restoring couple. Assuming that the system is rigid and that the canopy mass is lumped at the quarter chord point, the moment *M* about the wing quarter chord of the system may be written with reference to Figure 23:

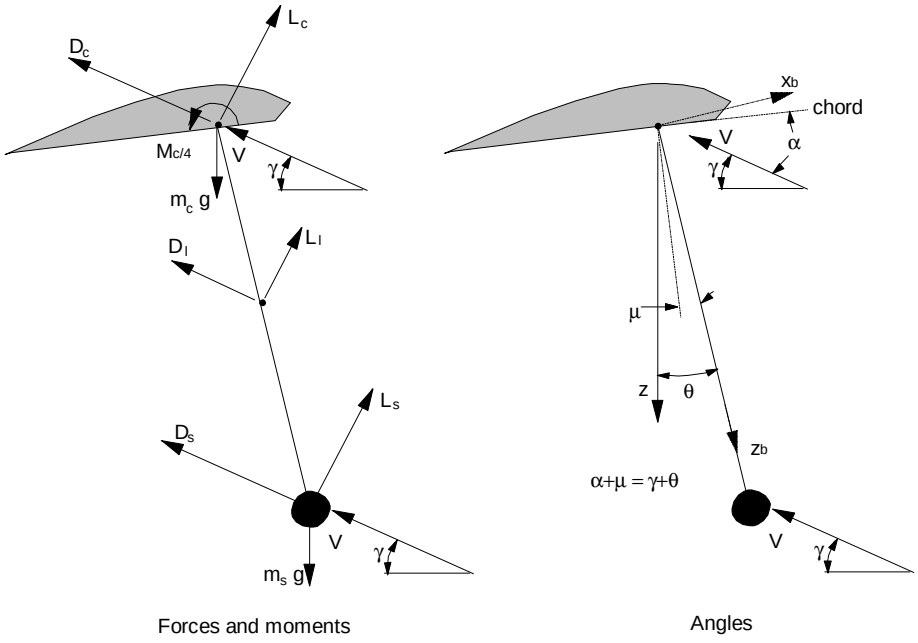

Figure 23 Definitions for static stability analysis

$$M = M_{c/4} + R\left[L_s \sin(a+m) - D_s \cos(a+m)\right] + \frac{R}{2}\left[L_l \sin(a+m) - D_l \cos(a+m)\right] - m_s g R \sin q \qquad (15)$$

where $M_{c/4}$ = pitching moment of the canopy about 25% chord point,
L_l = lift force acting on the suspension lines
L_s = lift force acting on the payload
D_l = drag force acting on the suspension lines
D_s = drag of the payload
m_s = mass of the payload
g = acceleration due to gravity
R = distance from the quarter chord point of the canopy to the payload,
and m = rigging angle as defined in Figure 23.

Line force is assumed to act normal to and at the mid-point of the line joining the 25% chord point to the payload. Therefore line drag and lift may be written:

$$C_{Dl} = \frac{ndR\cos^3(a+m)}{S}$$

$$C_{Ll} = -\frac{ndR\cos^2(a+m)\sin(a+m)}{S}$$

Writing equation (15) in coefficient form:

$$C_M = C_{MC/4} + \frac{R}{c}\left[C_{Ls}\sin(a+m) - C_{Ds}\cos(a+m)\right] + \frac{R}{2c}\left[C_{Ll}\sin(a+m) - C_{Dl}\cos(a+m)\right] - \frac{m_s gR\sin q}{½\,rV^2Sc}$$

or simplifying

$$C_M = C_{MC/4} + \frac{R}{c}\left[C_{Ls}\sin(a+m) - C_{Ds}\cos(a+m)\right] - \frac{R}{2c}\frac{nRd\cos^2(a+m)}{S} - \frac{m_s gR\sin q}{½\,rV^2Sc} \qquad (16)$$

Lift, drag and pitching moment data for a ram-air wing of A = 2.5 are shown in Figures 24-26.

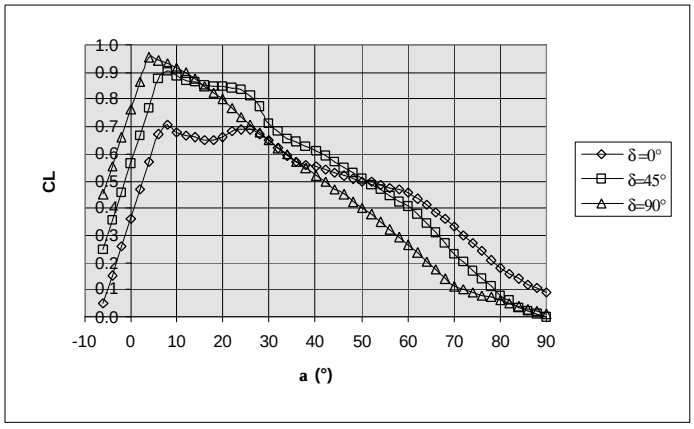

Figure 24 Lift coefficient for a ram-air wing without lines, A = 2.5

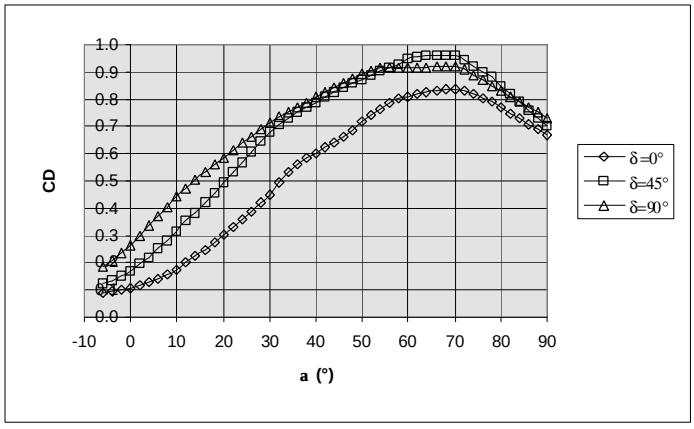

Figure 25 Drag coefficient for a ram-air wing without lines, A = 2.5

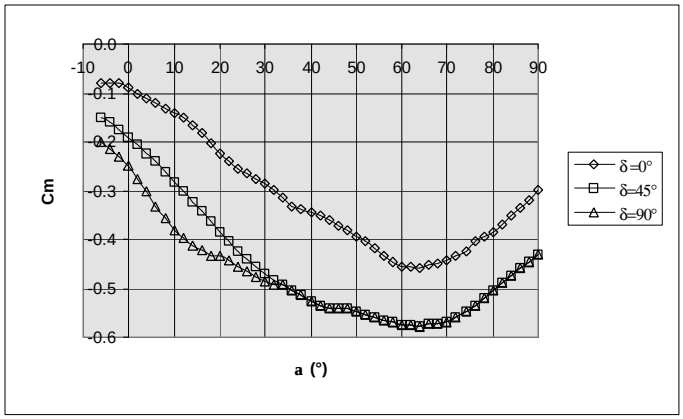

Figure 26 Pitching moment coefficient for a ram-air wing without lines, A = 2.5

The variation of pitching moment with rigging angle derived from equation (16) is illustrated in Figure 27. System parameters are S = 300 m^2, A = 2.5, R/b = 0.6, m_s = 5229 kg, n =270, d = 0.0025, C_{Ds} = 0.006, C_{Ls} = 0.

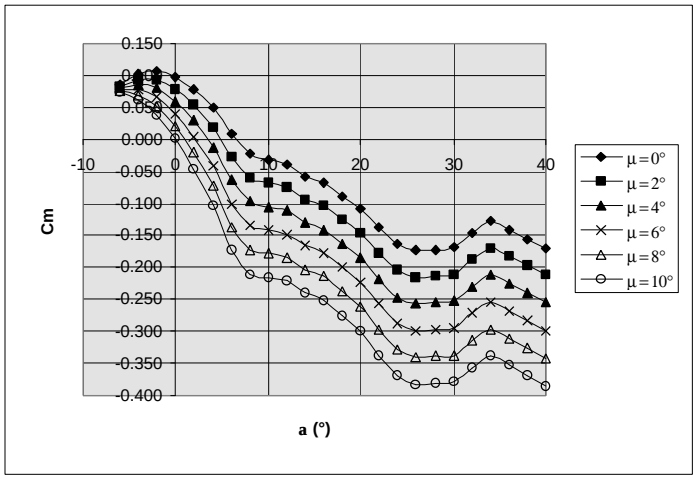

Figure 27 Pitching moment coefficient for a ram-air parachute with various rigging angles, S = 300m^2, A = 2.5, R/b = 0.6

It is clear that variation of m is an effective means of selecting the stable angle of attack, a, a wide range of stable values of a being available for fairly small changes in m. In this case the system will fly at a = 2.8° resulting in C_L = 0.5 if rigged with m = 5°. In this configuration C_D = 0.165, giving an L/D ratio of 3.03. Rigging the canopy with m too high results in a lower trim angle of attack and a fall off in performance; setting m too low may lead to the trim angle of incidence being beyond the stall, resulting in a considerable drop in performance. This sensitivity to rigging emphasises the need for accurate rigging using suspension lines with very low elasticity.

The effect of increasing line length to R/b = 1.0 is shown in Figure 28.

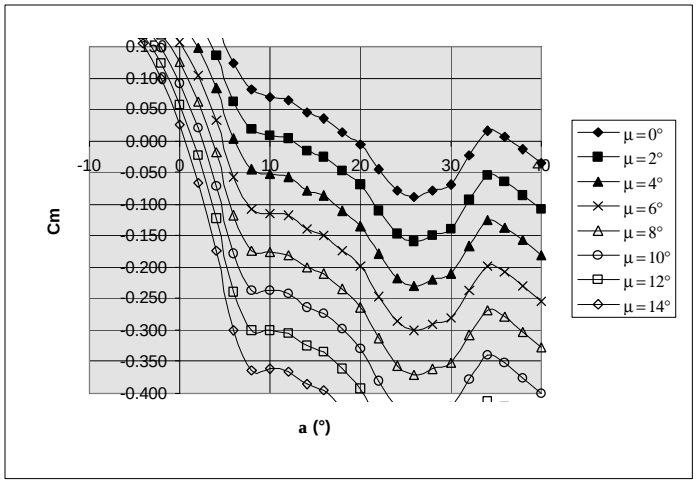

Figure 28 Pitching moment coefficient for a ram-air parachute with various rigging angles, S = 300m^2, A = 2.5, R/b = 1.0

With longer lines it is necessary to increase the rigging angle to m = 9.1° to attain the desired trim lift coefficient of 0.5. The parachute will fly at a = 2.9°, C_D = 0.187, giving an L/D ratio of 2.67. The magnitude of dC_m/da at C_m = 0 becomes greater with longer lines implying increased static stability.

Increasing aspect ratio also results in improved static stability the value of dC_m/da again increasing due to the greater line length.

6.2 Effect of trailing edge deflection

On a conventional wing deflecting plain flaps changes the camber of the section and results in increases of lift coefficient at a given incidence, maximum lift coefficient, profile drag and induced drag. Deflecting the trailing edge of a ram-air wing produces similar effects as is demonstrated in Figures 24-26.

The effect of flap deflection d to half and full brakes position on the system pitching moment about the wing quarter chord point is shown in Figures 29 and 30 for the standard system. The influence of flap deflection on the various flight parameters is shown in Figures 31, 32 and 33.

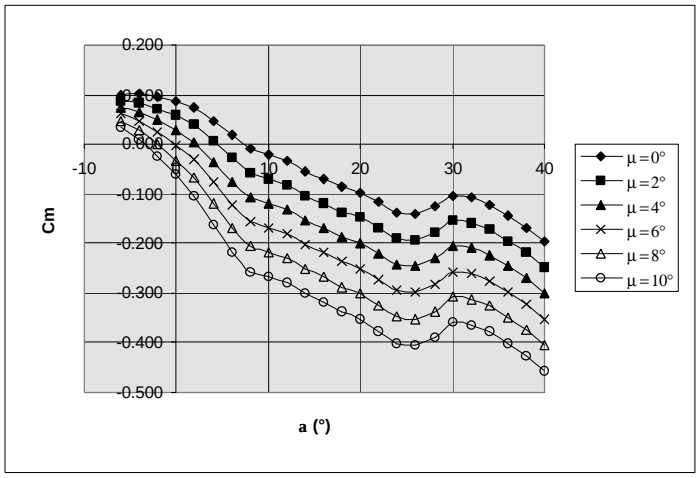

Figure 29 Pitching moment coefficient for a ram-air parachute with various rigging angles, S = 300m^2, A = 2.5, R/b = 0.6, d=45°

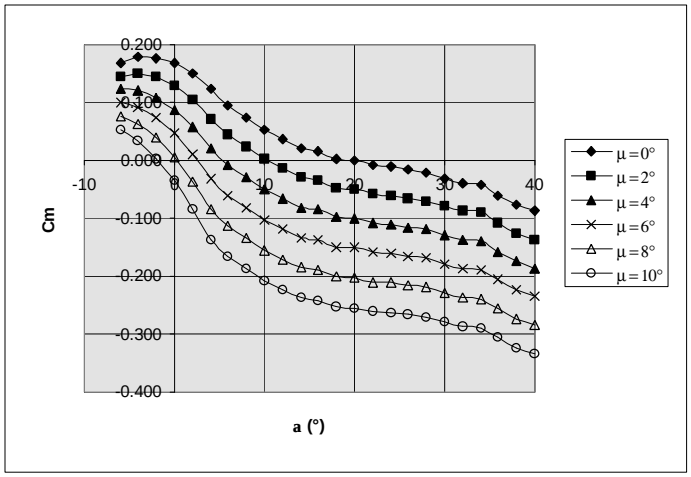

Figure 30 Pitching moment coefficient for a ram-air parachute with various rigging angles, S = 300m^2, A = 2.5, R/b = 0.6, d=90°

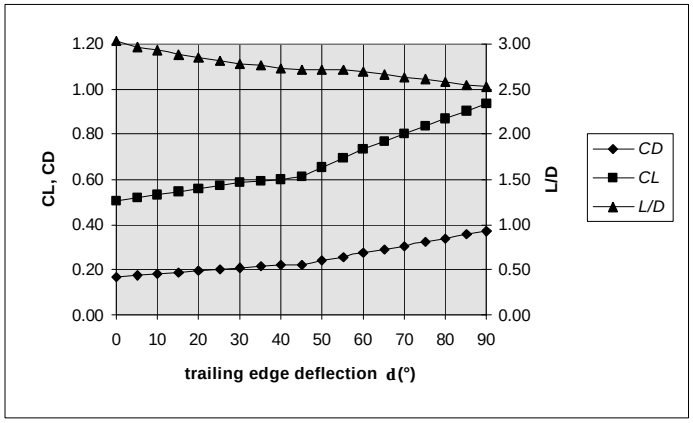

Figure 31 Influence of trailing edge deflection on lift and drag coefficients and lift to drag ratio for the standard system

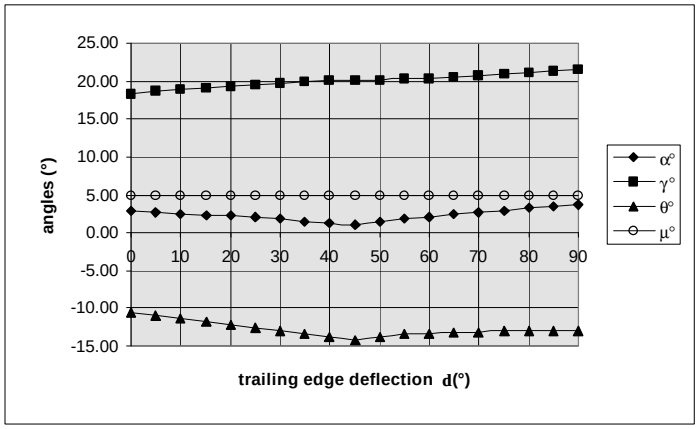

Figure 32 Influence of trailing edge deflection on trim values of a, $g$and q for the standard system

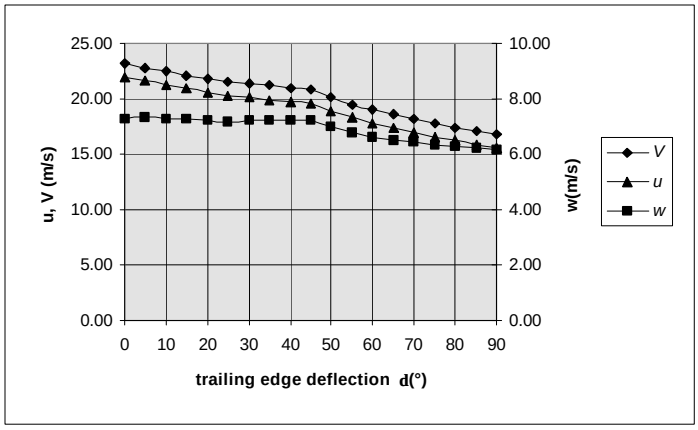

Figure 33 Influence of trailing edge deflection on flight velocities for the standard system

Deflection of the trailing edge results in only a small changes in trim angle of attack. C_L and C_D increase almost in proportion resulting in *L/D* reducing (*g* increasing) only slightly from 3.03 to 2.52 with *d* changing from 0° to 90°. The significant increases in lift and drag coefficients result only in reduced flight velocity. Thus, deflecting the trailing edge does not strongly influence glide angle for the standard system, γ changes only from 18.3° to 21.6°. Therefore, in this configuration controlling glide slope in zero wind conditions is not feasible.

This is not true for all rigging configurations. With increased line length, trailing edge deflection can result in a significant change in trim angle as shown in Figures 34 and 35. With the system rigged off-design with $m = 6°$ fully deflecting the trailing edge results in a shift of trim angle of attack from 3.8° to 36.3°.

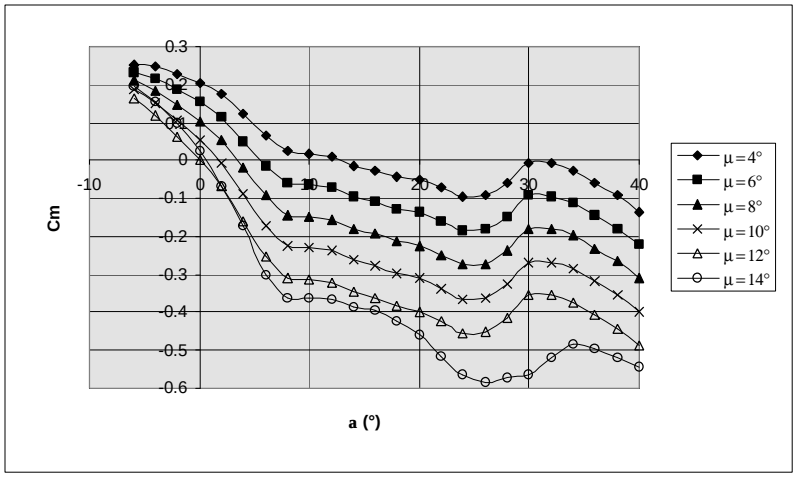

Figure 34 Pitching moment coefficient for a ram-air parachute with various rigging angles, $S = 300m^2$, $A = 2.5$, $R/b = 1.0$, $d = 45°$

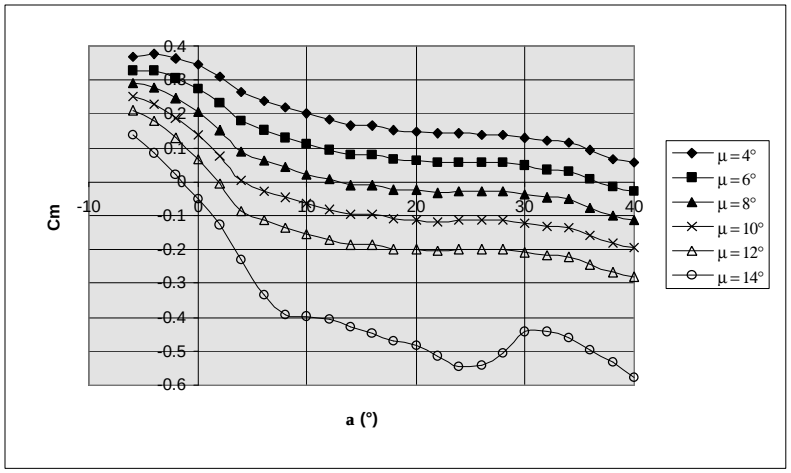

Figure 35 Pitching moment coefficient for a ram-air parachute with various rigging angles, S = 300m^2, A = 2.5, R/b = 1.0, d=90°

If the system is flying into the wind, as it ideally would be for landing, deflection of the trailing edge can cause a more significant change in glide angle for the standard system. This occurs because forward velocity decreases as $d$increases and the headwind has a proportionally greater effect. This is illustrated in Figure 36. With a 10 m/s headwind the glide angle can be adjusted by trailing edge deflection from 31° to 48°. The possibility to adjust glide slope is even greater for man carrying systems. This adjustment is used by jumpers in accuracy competitions.

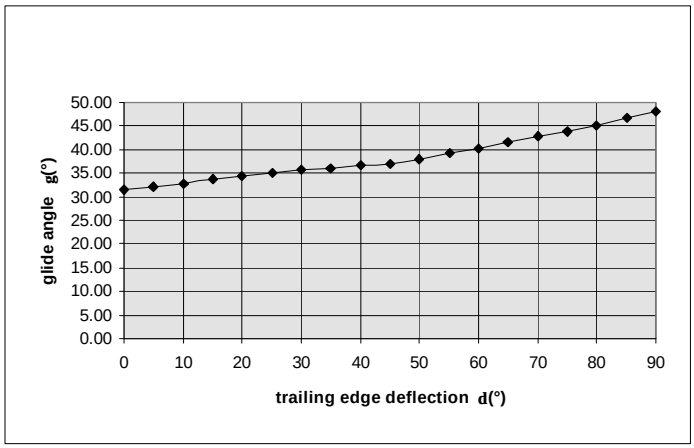

Figure 36 Influence of trailing edge deflection on glide angle for the standard system with a 10m/s headwind

7 RAM AIR PARACHUTE LONGITUDINAL DYNAMICS

7.1 General

In this section consideration is given to the dynamics of ram-air parachute flight. Dynamical analysis is important in that it can indicate conditions under which steady glide is rapidly achieved, and conditions where dynamic instability may occur or transient motions are only lightly damped. Of particular importance is the ability of the system to move smoothly from one state to another. This includes release of the trailing edge of the parachute following inflation, stall recovery, response to dynamic trailing edge deflection - glide path modification and the landing flare manoever - and gust response. Here motions are limited to the pitch plane. In the following section lateral control and stability will be discussed.

The dynamic stability model used to derive the results described in this seminar is detailed in Reference 3. It is important to note that inclusion of the added masses is the equations of motion is important in obtaining correct predictions. Added masses are derived in references 3 and 13.

The model is capable of simulating the effects on flight dynamics of changes in system parameters such as canopy size, line length, rigging angle, payload mass and aerodynamic characteristics and environmental parameters. In this section it is applied to review the response of a ram-air parachute system to control inputs and gusts and to evaluate the impact of variations in parachute size, payload mass, line length and altitude on system stability.

7.2 Longitudinal dynamics of small ram-air parachutes

Consider initially a small ram-air parachute system with the following parameters:

- S = 36 m^2
- A = 2.5
- R/b = 0.6
- m = 3.5°
- m_s = 217 kg
- C_{Ds} = 0.006

It is well known that small ram-air parachutes can perform an effective flare manoever to reduce landing velocity. This is shown in Figures 37 and 38. Flight is commenced at 400 m. Initially the parachute is in steady glide for three seconds, subsequently the trailing edge is deflected to the full brakes position over one second. During the first three seconds the system maintains a horizontal velocity of 13.3 m/s and a vertical velocity of 3.7 m/s. L/D is 3.6. The stable angle of attack is 2.9°, the payload is swung backward with q = -9.3° and the glide angle is 15.7°.

The short period during and immediately after control deflection simulates the flare manoever. The objective of a flared landing is to simultaneously reduce both horizontal and vertical velocity by increasing lift and drag. Referring to Figure 37 and 38, it is noticed that immediately following initiation of control deflection the canopy horizontal velocity falls rapidly with the payload deceleration lagging. The system therefore pitches up, with q eventually reaching 5.6° forward 1.8 seconds from control initiation. Glide angle reduces, attaining 7.2° coincident with maximum pitch forward. Following an initial slight reduction (predictable from static analysis for $d$up to 45°), a rises to 10° at maximum pitch forward of the payload. The vertical velocities of the canopy and payload, which are almost identical throughout the manoever, initially fall to 1.35 m/s before rising again to >4.0 m/s. The minimum vertical velocity occurs at maximum pitch forward which is the time at which the payload would ideally land. The horizontal velocity at this time is 10.7 m/s and has not reached its minimum value which occurs at the bottom of the backswing of the payload. When minimum horizontal velocity occurs vertical velocity has risen again to 3.0 m/s. The time between control initiation and ideal touchdown is 1.8 s with a height loss of 4.6 m.

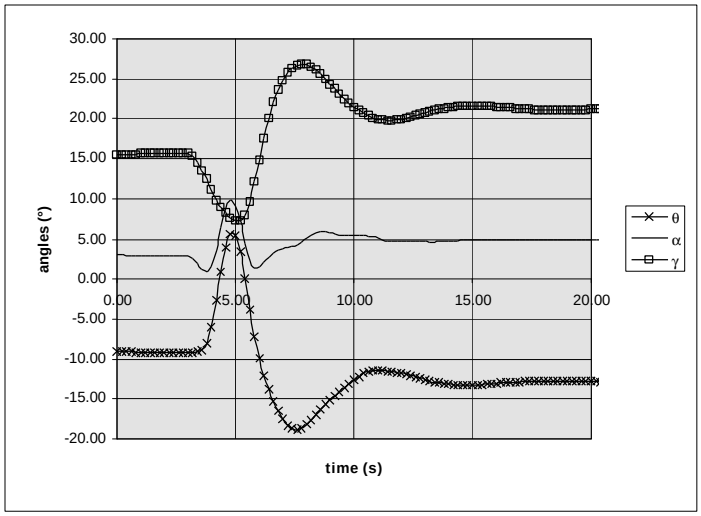

37 Response of ram air parachute to trailing edge deflection, S = 36m^2, R/b = 0.6, m_s =217kg, h=400m

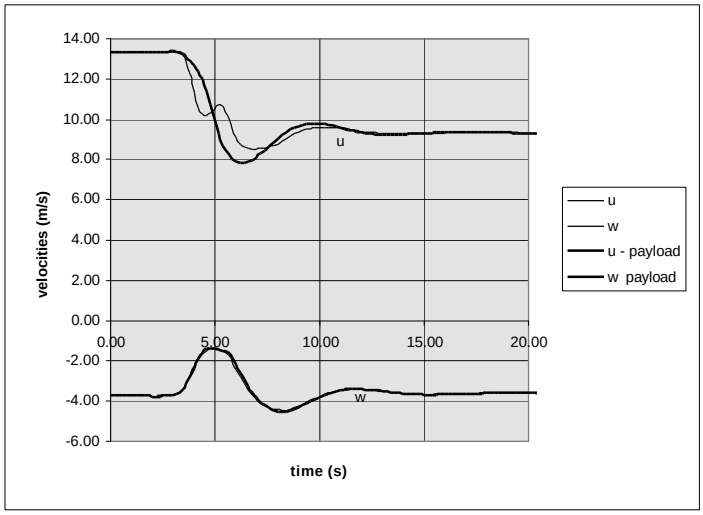

Figure 38 Response of ram air parachute to trailing edge deflection, S = 36m^2, R/b = 0.6, m_s =217kg, h=400m

It is clear that the flare is essentially a dynamic manoever. If control initiation is too early vertical velocity will be high, if too late horizontal velocity will be high. A headwind can significantly improve the quality of the landing. In this case, with a wind of 7.5 m/s, the ideal landing would result in a vertical velocity of 1.35 m/s and a horizontal velocity of only 3.2 m/s.

Subsequent to the simulated flare, a highly damped phugoid motion occurs. All disturbance is damped in 2 cycles, 12 seconds after control initiation. Steady gliding flight at full brakes follows with a = 4.7°, u =9.3 m/s, w = 3.6 m/s and L/D = 2.6.

7.3 Scaling effects

The small ram-air configuration clearly has good dynamic characteristics and in scaling up to large parachutes, appropriate to the PADS role, it is essential that these are retained. It is therefore useful here to digress in order to discuss scaling parameters. At first sight one may assume that a good option would be to maintain wing loading in

order to match flight speed. However there is another option. In considering general dynamic parachute motion, three non-dimensional parameters which influence parachute behaviour in unsteady motion regularly arise:

$\frac{m_s}{rD_0^3}$ mass ratio M_r

$\frac{V^2}{gD_0}$ Froude number F_r

$\frac{Vt}{D_0}$ dimensionless time t .

Mass ratio represents the ratio of payload mass to an air mass associated with the canopy. This parameter influences many unsteady parachute phenomena including inflation and wake recontact.

In classical hydrodynamics Froude number represents the ratio of fluid inertial forces to gravitational forces. For a parachute in steady descent:

$$krV^2D_0^2 = m_s g$$

where k is a constant ($pC_T / 8$).

Hence, substituting in the Froude number term for V^2, we obtain

$$F_r = \frac{1}{k} \cdot \frac{m_s g}{rD_0^2} \cdot \frac{1}{D_0 g} = \frac{1}{k} \cdot \frac{m_s}{rD_0^3}$$

Thus for a parachute in steady descent Froude number is equivalent to mass ratio and we may use either parameter.

Because, in unsteady motion, time is a parameter, a group emerges from dimensional analysis relating time interval to a characteristic time for the parachute. Dimensionless time, t, is defined as velocity divided by a characteristic length for the parachute:

$$t = \frac{V}{D_0}$$

In analysing unsteady behaviour of systems of different scales this parameter is useful to compare response times.

Consider the small ram-air parachute system defined above. The wing loading for the system, m_s/S, is 6.02 kg/m^2. Mass ratio, defined for a for ram-air parachutes as $m_s/ r S^{1.5}$, is 0.82. Scaling up to a 300 m^2 wing on the basis of wing loading would give a payload mass of 1808 kg and matching mass ratio gives 5229 kg. Other parameters for the scaled up system are as follows:

- S = 300 m^2
- A = 2.5
- R/b = 0.6
- m = 5°
- C_{Ds} = 0.006

The time to deflect the trailing edge is also scaled on the dimensionless time basis. For the small system:

steady glide velocity = 13.9 m/s
representative length = $S^{½}$ = 6.0 m
deflection time = 1.0 s

thus

$$\text{dimensionless time of pull} = t = \frac{Vt}{L} = \frac{13.9 \times 1.0}{6.0} = 2.32$$

For the payload scaled on mass ratio, steady glide velocity is 23.4 m/s, and the representative length is 17.3m. Deflection time should therefore be 1.7s. That is time is scaled by a factor of 1.7 between the two systems.

To evaluate the two scaling parameters the test flight used for the small system is repeated for the scaled up system.

Figures 39 and 40 show the response of the system scaled on the basis of mass ratio. The response is qualitatively very similar to the small system. An effective stall is achieved with the subsequent motion well damped.

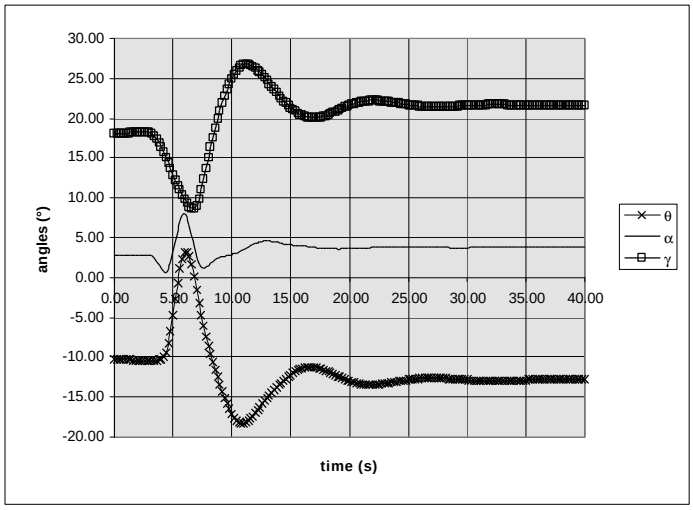

Figure 39 Response of ram air parachute to trailing edge deflection, S = 300m^2, R/b = 0.6, m_s =5229kg, h=400m

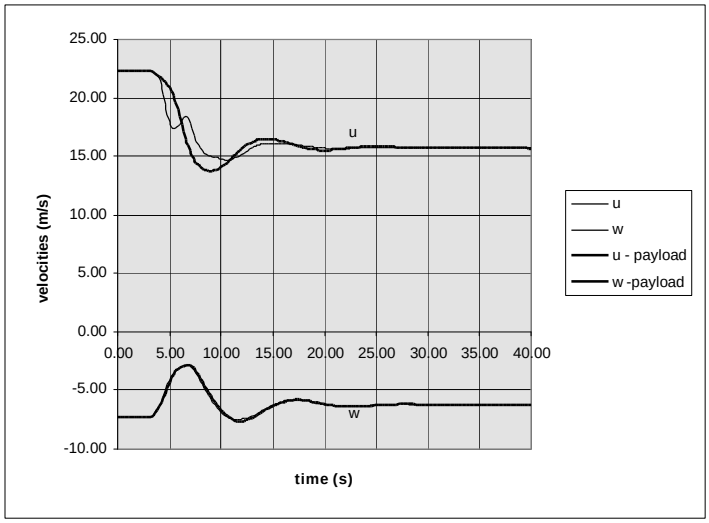

Figure 40 Response of ram air parachute to trailing edge deflection, S = 300m^2, R/b = 0.6, m_s =5229kg, h=400m

During the first three seconds the system flies at a horizontal velocity of 22.3 m/s and a vertical velocity of 7.3 m/s. *L/D* is 3.0. The stable angle of attack is 2.9°, the payload is swung backward with q = -10.3° and the glide angle is 18.2°. During the flare the parachute pitches up to a maximum q of 3.2°, slightly after which vertical velocity is

reduced to 2.8 m/s and horizontal velocity to 16 m/s. Minimum vertical velocity is achieved 3.8 seconds after control initiation. Height loss during the manoever is 18 m. It is worthy of note that the ratio of horizontal velocity at flare to initial horizontal velocity is 72% and the ratio of vertical velocities is 38%, compared with 79% and 36% for the small system. System response to maximum pitch up was 1.77 times that for the small system - close to the predicted ratio. Motion after flare is favourable with all disturbance damped within two cycles. Phugoid cycle time is 10.8 s compared to 6.5 s for the small system; a ratio of 1.7. The performance of the large system scaled on the basis of mass ratio is thus very close to the small prototype.

Figures 41 and 42 show the performance for the system scaled on the basis of wing loading. The response to control input is somewhat different. The flare manoever is acceptable but weaker with less pitch up of the payload. The subsequent motion is a lightly damped oscillation of pitch angle and angle of attack of period 6.3 s.

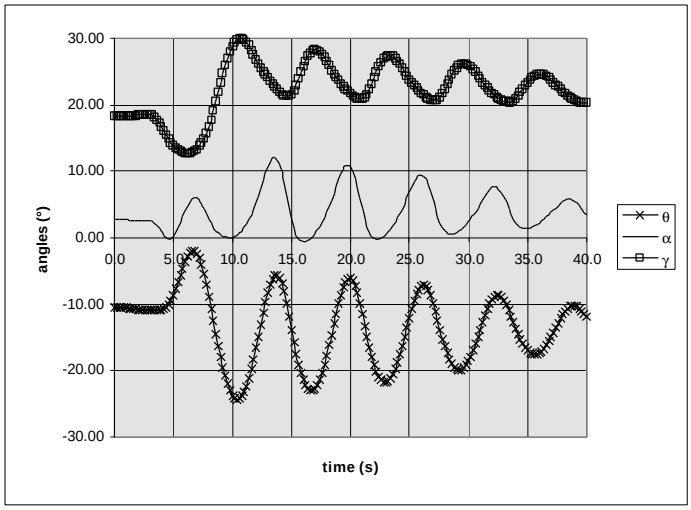

Figure 41 Response of ram air parachute to trailing edge deflection, S = 300m^2, R/b = 0.6, m_s =1808kg, h=400m

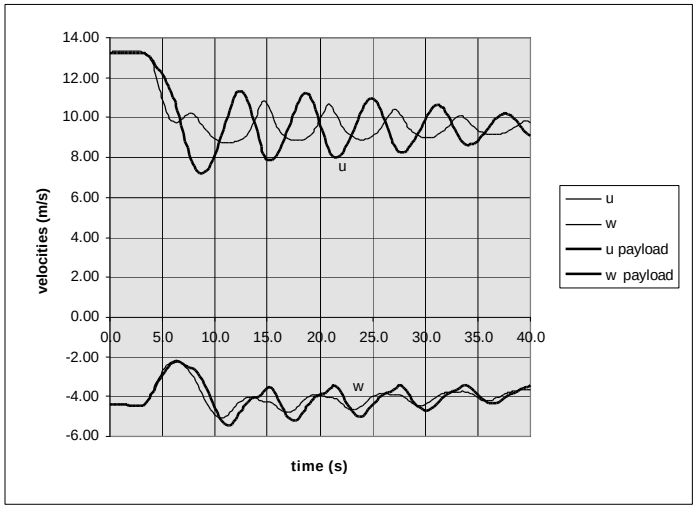

Figure 42 Response of ram air parachute to trailing edge deflection, S = 300m^2, R/b = 0.6, m_s =1808kg, h=400m

For the first three seconds of steady flight the system glides at a horizontal velocity of 13.3 m/s and a vertical velocity of 4.4 m/s and L/D is 3.0. The stable angle of attack is 2.7°, the payload is swung backward with q = -10.8° and the glide angle is 18.2°. In the flare the parachute only pitches to q of -2.0° at which time vertical velocity is reduced to 2.2 m/s and horizontal velocity to 10.0 m/s. Minimum vertical velocity is achieved 3.6 seconds after control initiation with height loss 10 m. Vertical velocity is only reduced to 50% the initial value

and horizontal velocity is reduced to 75% of the steady glide value. The poorly damped pitching motion after simulated flare would be of concern for a PADS operation since it would indicate that this configuration is sensitive to control inputs and gusts and would give unpredictable performance.

It can be demonstrated that the effect identified is related to mass ratio, and not some other feature of the configuration, if the simulation of the system scaled on the basis of wing loading is repeated with the parachute flying at high altitude such that mass ratio is also matched. This occurs at an altitude of 10,000 m. Figures 43 and 44 show that the performance is now identical to the system originally scaled on mass ratio.

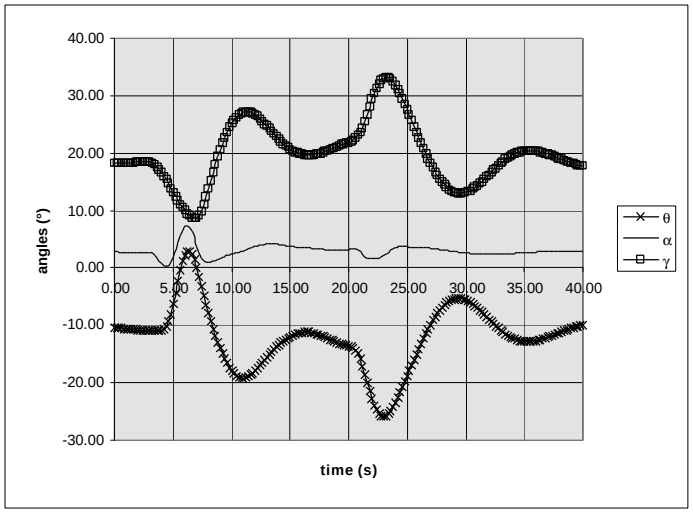

Figure 43 Response of ram air parachute to trailing edge deflection, S = 300m^2, R/b = 0.6, m_s =1808kg, h=10,000m

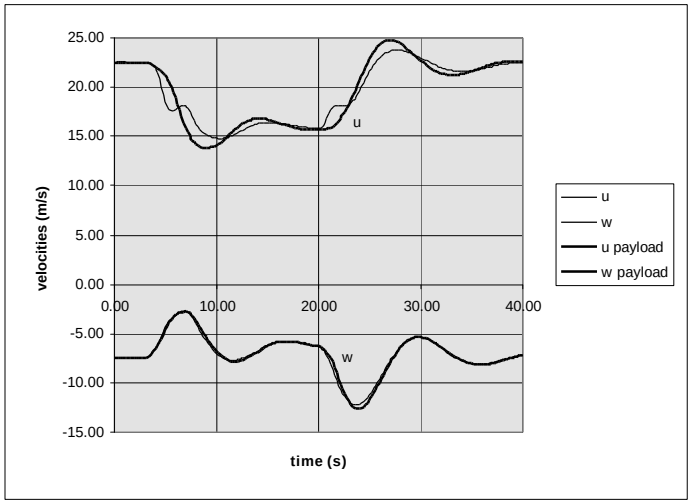

Figure 44 Response of ram air parachute to trailing edge deflection, S = 300m^2, R/b = 0.6, m_s =1808kg, h=10,000m

Thus to match dynamic performance of ram air parachutes scaling must be on the basis of mass ratio.

7.4 Effects of trailing edge release

During inflation the trailing edge of ram-air parachutes are retained in the full brake position to prevent surge during inflation. The ability to smoothly transition from this state to full glide is essential to PADS. The standard large system was subjected to a simulated flight with brakes fully applied over 1.7 seconds after 3 seconds of gliding flight, and released over 1.7 seconds after 20 seconds of flight. The results are shown in Figures 45 and 46.

- $S = 300\text{m}^2$
- $A = 2.5$
- $R/b = 0.6$
- $m = 5°$
- $m_s = 5229$ kg
- $C_{Ds} = 0.006$

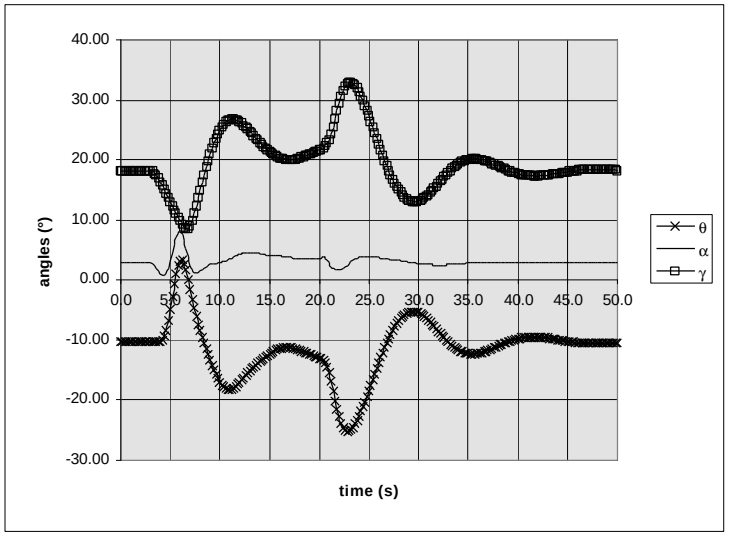

Figure 45 Response of ram air parachute to trailing edge deflection and release, $S = 300\text{m}^2$, $R/b = 0.6$, m_s =5229kg, h=500m

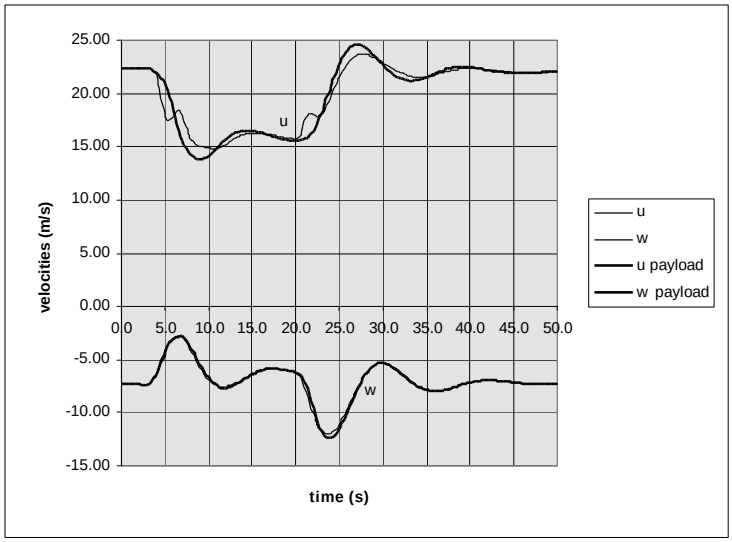

Figure 46 Response of ram air parachute to trailing edge deflection and release, $S = 300\text{m}^2$, $R/b = 0.6$, m_s =5229kg, h=500m

As the brakes are released the canopy accelerates rapidly with the load lagging. The system pitches down, eventually reaching q = -25°. Perturbation of angle of attack is very small. As the system dives and accelerates both vertical and horizontal velocity increase. When the payload swings forward again vertical velocity rapidly recovers to its steady glide value. Subsequent oscillations are highly damped. The ability to effect a good transition is thus demonstrated.

7.5 Effects of gusts

The effect of a 7.5m step tail gust on the standard large system is shown in Figures 47 and 48.

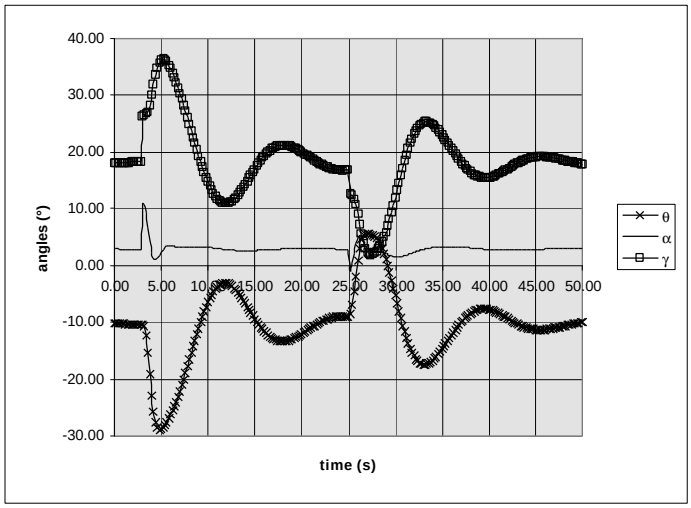

Figure 47 Response of ram air parachute to a step gust, S = 300m^2, R/b = 0.6, m_s =5229kg, h=500m

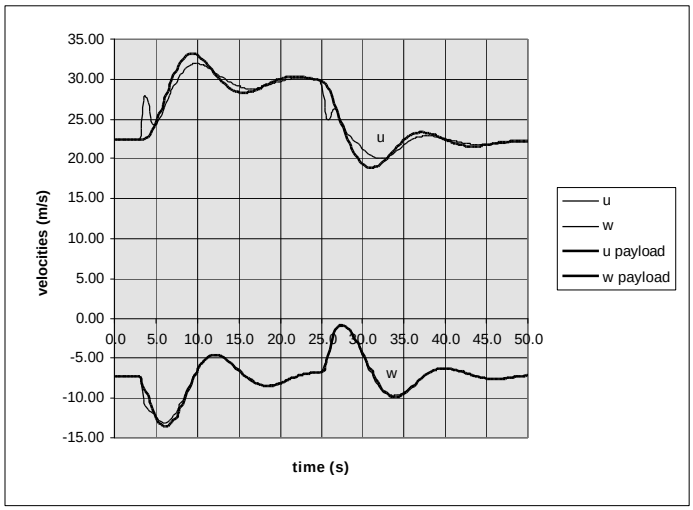

Figure 48 Response of ram air parachute to a step gust, S = 300m^2, R/b = 0.6, m_s =5229kg, h=500m

As the gust hits the parachute at time 3 seconds the response shown is similar to the release of brakes. The system pitches down rapidly and accelerates to recover the lost lift. Rate of descent initially rises but recovers as the payload pitches forward and the parachute glides out of the dive. Again a variations are only very transient. Following the gust, classical damped phugoid motion occurs with a constant. As the gust ceases at 25 seconds the effect is the equivalent of a head gust. The canopy responds by decelerating rapidly. The payload lags and the system pitches up. Rate of descent transiently falls to almost zero with the additional lift before the system pitches

down and steady glide is re-established. With the standard system gusts are accommodated with the resulting perturbations rapidly damped.

7.6 Effect of line length on longitudinal performance

To investigate the effect of line length on dynamic performance, the standard large system was modelled with line length increased to R/b = 1.0. The results are shown in Figures 49 and 50.

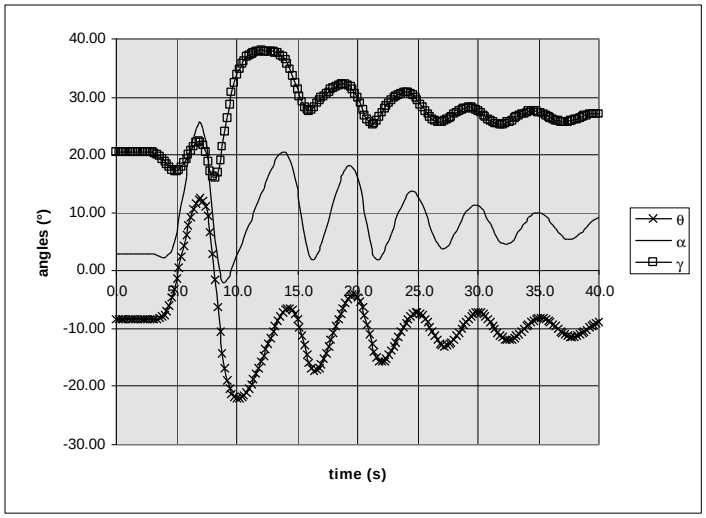

Figure 49 Response of ram air parachute to trailing edge deflection, S = 300m^2, R/b = 1.0, m_s =5229kg, h=400m

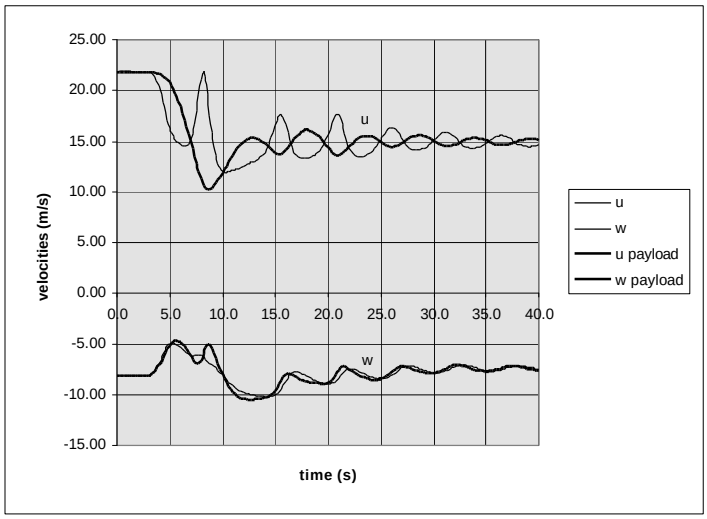

Figure 50 Response of ram air parachute to trailing edge deflection, S = 300m^2, R/b = 1.0, m_s =5229kg, h=400m

The system is initially established in a steady glide with u = 21.8 m/s, w =8.1 m/s and L/D = 2.7. The flare is poor with minimum vertical velocity occurring 1.8 s before maximum pitch up. Vertical velocity is only reduced to 58% of the initial glide velocity with horizontal velocity at this time still 90% of the steady glide figure. At maximum pitch up horizontal velocity is 15 m/s (69% of the steady glide value) but rate of descent has risen to 6.2 m/s (77% of the steady glide value). The perturbation in angle of attack is large with α reaching 25°; well beyond the stall. Recovery from the manoever is also poor with a sustained pitching motion ensuing. The poor performance is

related to the increased lag between canopy and payload response. Clearly then, increased line length not only reduces glide performance but also compromises longitudinal stability.

7.7 Effect of rate of retraction of trailing edge on flare

It is obviously easier to design retraction devices which do not have to deflect the trailing edge very rapidly. The impact of much slower trailing edge deflection on the effectiveness of the flare of the standard large system is therefore simulated. Figures 51 and 52 show the results of control actuation over 5 seconds.

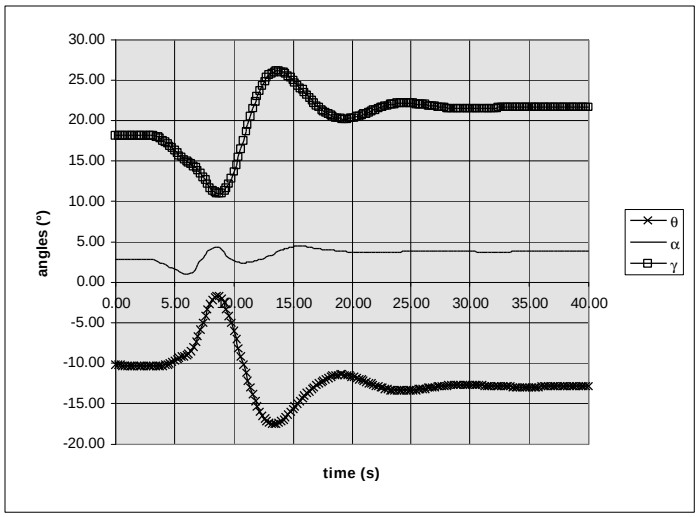

Figure 51 Response of ram air parachute to slow trailing edge deflection, S = 300m^2, R/b = 0.6, m_s =5229kg, h=400m

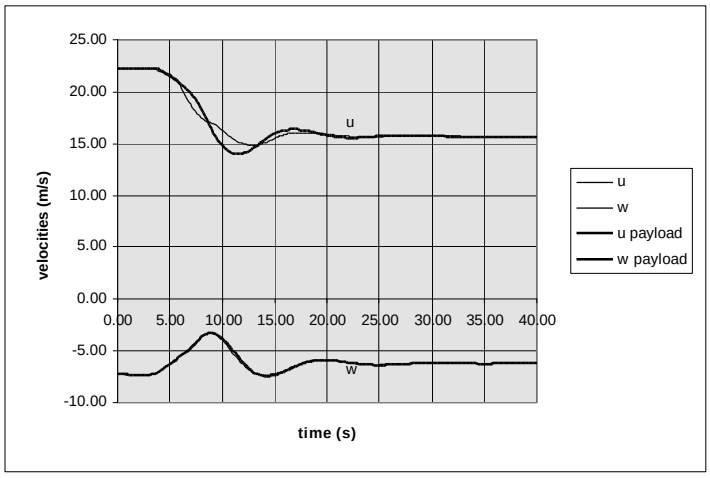

Figure 52 Response of ram air parachute to slow trailing edge deflection, S = 300m^2, R/b = 0.6, m_s =5229kg, h=400m

Again glide is established with u = 22.3 m/s and w = 7.3 m/s. Response of the system to control deflection is slower and pitch up of the system is less pronounced, with q only reaching -1.7°, 5.6 seconds after the start of control movement. At this time vertical velocity is at a minimum at 3.3 m/s, 45% of the initial value and horizontal velocity is 17.2 m/s, 77% of the initial value. Flare is therefore seen to be less effective with slower application of brakes but may still be acceptable. A low vertical velocity is still achieved and horizontal velocity is only 1.2 m/s greater than with rapid trailing edge deflection, a small percentage of the overall forward speed.

7.8 Summary

⇒ Acceptable longitudinal stability is achievable for large parachutes appropriate to the PADS role but scaling must be on the basis of mass ratio. Mass ratios in the range of 0.8 are recommended but severely adverse dynamics does not appear to occur above $M_r = 0.4$.

⇒ Increasing altitude increases mass ratio and therefore stability.

⇒ Increasing mass for a given canopy size increases stability.

⇒ Increasing line length is destabilizing.

⇒ Effective reduction in vertical velocity by the flare manoever is achievable at the recommended mass ratio, but residual horizontal velocities increase with system size: 10.7 m/s for a 36 m^2 wing, 16 m/s for a 300 m^2 wing and > 20 m/s for a 1000 m^2 wing.

8 RAM-AIR PARACHUTE LATERAL MOTION

8.1 General

The most important aspects of lateral motion for PADS are predictable turns and lateral dynamic stability.

In analysing lateral motion, a model based on the equations set out by Doherr [24] has been used. Aerodynamic data were derived from references 3 and 14. The axes and definitions are shown in Figure 53.

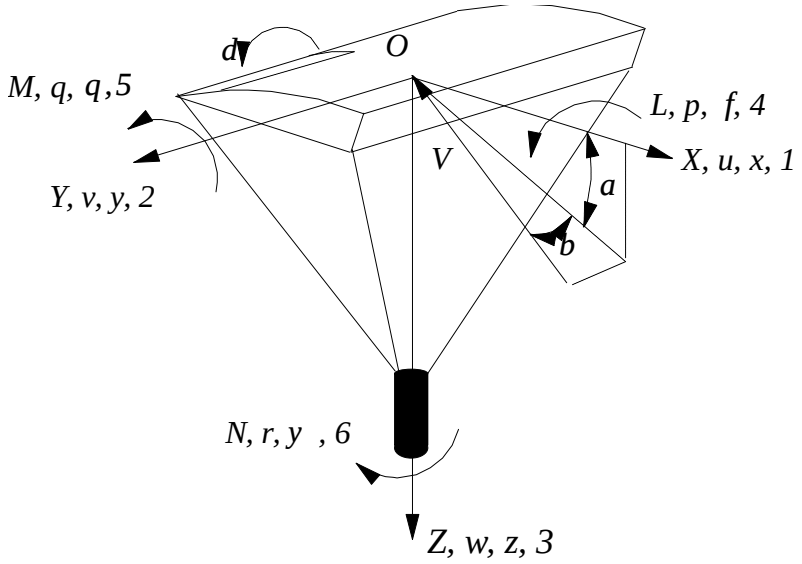

Figure 53 Definition of ram-air parachute axes

8.2 Turn Maneuver

Turns are initiated on ram-air parachutes by deflection of all or part of the canopy trailing edge on one side of the canopy. As discussed in the section on longitudinal static stability, deflection of the trailing edge of the wing increases the camber of the section and results in increases of lift coefficient at a given incidence, maximum lift coefficient, profile drag and induced drag. In response a trailing edge deflection, δ, the wing initially yaws in the positive direction. The lift caused by the deflection creates an adverse rolling moment. Centrifugal forces on the payload roll the wing in the correct direction and sustain the turn.

Of interest for PADS is achievable rates of turn, so first consider steady turning flight. The equations of motion of the system in body axes for about the yaw and roll axes in steady turning flight are:

$$qSb(C_{n_d} d + C_{nb} b + C_{nr} \frac{rb}{2V}) = (a_{22} - a_{11})uv - a_{13}vw + a_{26}ur \qquad (17)$$

$$qSb(C_{l_d} d + C_{lb} b + C_{lr} \frac{rb}{2V}) - m_s gR \sin f \cos q = -(m_s R + a_{15})ur + a_{13}uv + (a_{33} - a_{22})vw - (a_{26} + a_{35})wr \qquad (18)$$

where C_{n_d} = yawing moment coefficient due to control deflection;
C_{nb} = yawing moment coefficient due to sideslip;

C_{nr} = yaw damping coefficient due yaw rate;
$C_{l\,d}$= rolling moment coefficient due to control deflection;
C_{lb} = rolling moment coefficient due to sideslip;
C_{lr} = roll damping moment coefficient due to yaw rate;
r = yaw rate (rad/s)
a_{ii} = are the added masses referred to the axes defined in Figure 53.

Considering equation 17 :

a_{13} and a_{26} are small;
$a_{11} \approx a_{22} \approx$ the mass of air enclosed in the canopy;

and therefore the right hand side of the equation is approximately zero.

On the left hand side of the equation, for wings with zero sweep, $C_{nb} = 0$ [25]. We are therefore left with:

$$(C_{n\,d}\,d + C_{nr}\,\frac{rb}{2V}) = 0$$

or

$$r = -\frac{C_{n\,d}}{C_{nr}} \cdot \frac{2V}{b}\,d \qquad (19)$$

Rate of turn, for a given trailing edge deflection, is increased by velocity. The larger the parachute, the lower the turn rate for a given flight velocity and deflection. With values for $C_{n\,d}$ and C_{nr}, a good approximation for rate of turn, r, as a function of trailing edge deflection is available. Reference [25] proposes that

$$C_{nr} = -\frac{C_D}{6}$$

For a typical ram air parachute operating at a design lift coefficient of 0.5 with glide ratio 3:1 then $C_D = 0.167$, and $C_{nr} = 0.028$.

Assuming that the yawing moment produced by trailing edge deflection is entirely due to the difference in drag on each side of the wing, then from Figure 54 we can write:

$$C_{n\,d} = \frac{l\bar{y}}{b^2}\,\frac{dC_D}{d\,d}$$

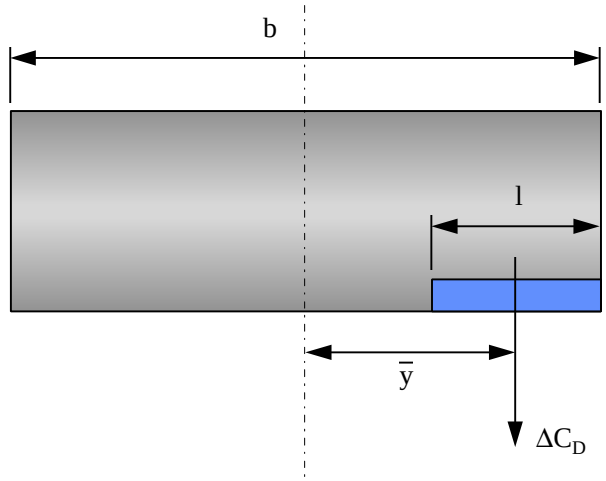

Figure 54 Yawing moment on ram-air wing

where $\frac{dC_D}{d\,d}$ = rate of change of drag with deflection of the complete trailing edge at the design angle of attack.

Further, assume the control lines act on the outer half of each side of the wing then

$$C_{n\,d} = \frac{3}{32}\frac{dC_D}{d\,d}$$

From Figure 26:

$$\frac{dC_D}{d\,d} \approx 0.11 \text{ per radian}.$$

Therefore $C_{n\,d} = 0.01$.

Substituting into equation (19) we finally have:

$$r = 0.71 \cdot \frac{V}{b}\,d \qquad (20)$$

Thus for a typical large PADS system with b = 30 m and V = 20 m/s only 21° (0.366 rad) trailing edge deflection is needed to produce a turn rate of 10°/s (0.175 rad/s). The radius of turn R_c for this case is therefore

$$R_c = \frac{u}{r} = \frac{V\cos g}{r} = \frac{19.0}{0.175} = 108 \text{ m}$$

Consider now equation 18. The added mass terms are negligible with the exception of $(a_{33}\text{-}a_{22})vw$. This term , however, has a value in the absence of acceleration and would be included in wind tunnel measured aerodynamic data as a part of C_{lb}. It therefore may also be neglected. On the right hand side of the equation the aerodynamic terms are an order of magnitude smaller than the gravitational term an thus to a first approximation:

$$m_s gR\sin f\cos q = (m_s R)ur$$

or since q is small $\quad f = \sin^{-1}\frac{ur}{g}$

So the motion of a ram-air parachute system simplifies to that of a pendulum undergoing curved motion. The sine of the angle of bank is approximately the ratio of the centrifugal acceleration and gravitational acceleration. For the case above

$$f = \sin^{-1}\frac{19.0 \times 0.175}{9.81} = 19.8°$$

8.3 Lateral instabilities

Doherr [26] shows that large ram-air parachutes are undamped in spiral divergence and only lightly damped in Dutch roll.

Spiral divergence occurs when a turn in one direction is sustained. Rate of turn, velocity and bank angle increase and the path helix steepens. Mathematical modelling indicates that slow turns can be sustained but above a certain turn rate spiral divergence develops. Divergence seems to occur if the centrifugal acceleration ur exceeds a critical value. Modelling suggests that the boundary is approximately 4 m/s^2 or when bank angle exceeds 24°. For a

typical large PADS system with b = 30 m and V = 20 m/s this criterion means that sustained turn rate should be kept less than 0.2 rad/s or 11.5°/s. Moreover, since turn rate for a given deflection and speed increase with the problem of spiral divergence would seem to be exacerbated. Since the analysis is tentative sustained turns should be avoided. Therefore, if a holding pattern close to the target is part of the control strategy, a figure of eight is better than a sustained turn in one direction.

The Dutch roll mode seems similar to the phugoid mode in that shorter suspension lines and increased mass ratio are stabilizing.

9 INFLATION OF RAM-AIR PARACHUTES

9.1 General

Analysis of films showing the inflation of ram-air parachutes reveals that the canopy initially inflates in a manner similar to a conventional parachute, until it first reaches normal flying size, with little cell inflation. Subsequently, it starts to collapse and pitches forward. As the pitching motion occurs the cells inflate and the parachute begins to fly.

Without inflation control ram-air parachutes develop high inflation loads. This is not surprising since the initial inflation phase is extremely rapid. Some trials data has indicated dimensionless inflation times $V_s t_i/D_0$ of approximately 2.0 -5.0, where V_s is the snatch velocity, t_i is the inflation time and D_0 is the diameter of a circle equal in area to the planform area of the parachute. These times should be compared to values of 10.0 for conventional, man carrying, circular parachutes.

In addition to the opening load, a second force peak can occur because of the lift and drag forces generated during the rapid pitch forward phase of inflation.

Because of these high loads a reefing device is employed to reduce the initial opening load; and the second peak load during the rapid pitch forward is prevented by initial trailing edge deflection.

9.2 Reefing Techniques

Early ram-air parachutes used a variety of reefing techniques including the "ropes and rings technique". The pilot chute was attached to a bridle which was routed down to the centre of the canopy and then passed outboard through a series of rings along the canopy surface. The bridle thus acts as a drawstring, resisting the spanwise inflation of the canopy. Upper and lower surface versions of this technique were used. In the latter the bridle passed through grommets in the upper and lower surfaces of the canopy to rings on the lower surface. This method is more effective than the upper surface version since lower forces are needed for positive control of inflation.

Modern canopies for man carrying purposes, however, usually use slider reefing. The slider comprises four rings each of which passes round one of the four sets of suspension lines from the four risers. The lines are either located at the corners of a square of fabric. The slider area is typically 2% of the canopy area. At the start of the inflation the slider is positioned at the top of the lines adjacent to the canopy, effectively reefing the canopy. During inflation the tension in the lines forces the slider down toward the risers. This motion is resisted by air drag on the slider and thus inflation rate is controlled. On some systems the pilot chute is attached to a webbing cross and downward motion of the slider is resisted by the pilot chute drag.

With the increasing size of ram-air parachutes for cargo and space missions other reefing techniques have been developed. Puskas [14] describes the use of a sail slider for a 3000 ft^2 system. The ARS uses a Pioneer proprietary system called Mid-Span Reefing. The effect of this system is to completely remove sets of reefed cells from the airflow by compressing them spanwise. A fringe benefit of this system is that it enables the reefed cells and their rigging lines to be fabricated from lighter materials than the first stage cells since they never see the high loads associated with the deployment dynamic pressure. Weight savings in excess of 30% are claimed. Reefing ratios used on the ARS were 25.9% and 48.1%.

9.3 Inflation analysis

The complex inflation characteristics of a ram-air parachute with reefing make analysis of this phase difficult. Engineering calculations may be made using semi-empirical methods. The following approach is typical and works reasonably well.

Unsteady parachute inflation force data obtained from experiments are found to be well correlated when plotted in the form of force coefficient $C_F = F / qS_0$ versus dimensionless time.

This implies that:

- inflation force coefficient is independent of mass ratio and Froude number and is a function only of dimensionless time; that is a given parachute type has a dimensionless inflation force - time signature;
- inflation time occurs in a fixed dimensionless time $t_0 = V_s\, t_i / D_0$.

The dimensionless inflation time and inflation force time signature can be extracted from a limited number of tests.

The majority of simple semi-empirical methods such as those of Knacke [27], Ludtke [28] and Lingard [29] rely, with some individual refinements, on these assumptions.

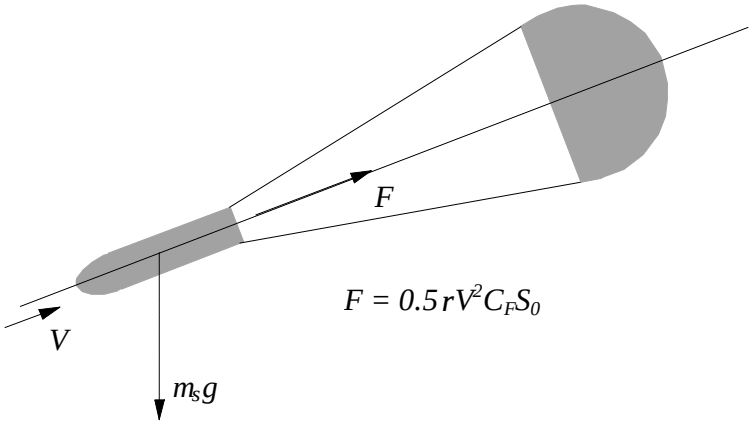

Figure 55 Schematic diagram of inflating parachute

The equations of motion of the system shown in Figure 55 may be written:

$$m_s \frac{dV}{dt} = m_s g \cos q - \frac{1}{2} r V^2 C_F(t) S_0$$

$$\frac{dq}{dt} = -g \frac{\sin q}{V} .$$

where $C_F(t)$ is the unique force coefficient versus dimensionless time function.

Note that

$$t = \frac{V_s}{D_0}(t - t_i)$$

and

$$t_0 = -\frac{V_s t_i}{D_0} .$$

This yields a set of four equations which, for known $C_F(t)$ and t_0 can be easily solved for V and q allowing inflation force, F, to be calculated. This method works well for slider reefed parachutes. Force coefficient may be approximated by:

for $t <= t_i$ $\quad C_F = 1.5 \times \left(\frac{t}{t_i} \right)^3$

for $t > t_i$ $\quad C_F = 1.0$.

Dimensionless inflation time, t_0 , is in the range 12 -18 depending on the slider design, with 14 a good starting point.

This model does not explicitly take added mass into account. Indeed, in using experimentally measured dimensionless force time curves as a basis for the model, it is assumed that added mass is automatically accounted for. Added masses for parachutes are significant, often being much larger than the suspended mass. The forces due to added mass effects depend on the rate of change of added mass and on the magnitude of the acceleration. During the inflation process, large rates of change of added mass occur. This is particularly true for rapidly inflating parachutes. If mid-span reefing is used, inflation between stages can be rapid since when the parachute is not reefed free, unrestrained inflation takes place. To allow for this a different type of model, in which added mass is explicitly treated, is useful.

Assume that the drag coefficient of the parachute is constant and the profile drag is simply a function of the parachute's instantaneous projected diameter. Additionally assume that there is an added mass, a_{11} , associated with the parachute which is also a simple function of the instantaneous projected diameter. The equations of motion of the inflating parachute system from Figure 55 may be represented by:

$$m_s \frac{dV}{dt} = m_s g \cos q - \frac{1}{2} r V^2 C_D S' - a_{11} \frac{dV}{dt} - V \frac{da_{11}}{dt}$$

$$\frac{dq}{dt} = -g \frac{\sin q}{V} .$$

For inviscid flow the added mass of a disc in the direction of its axis of symmetry is:

$$a_{11} = r \frac{D^3}{3}$$

To complete the model a function for the variation of projected diameter against time and a value for C_D are required. For ram air parachutes

$$D = D_0 \left(\frac{t}{t_i} \right)^{1.5}$$

where $\quad D_0 = \left(\frac{4S}{p} \right)^{0.5}$.

Also $\quad S' = \frac{pD^2}{4}$.

Typical steady state force coefficient for a ram-air parachute with full brakes is 1.0.

Finally the inflation time for these parachutes may be approximated by:

for free inflation: $\quad t_i = \frac{3.5 D_0}{V_s}$

for slider reefing: $t_i = \frac{14 D_0}{V_s}$.

With this type of model the inflation factor is automatically generated. This model was applied to the slider reefed MC-4 parachute with 163 kg suspended mass deployed at 72m/s. The results are compared with test in Figure 56. The match obtained is reasonable.

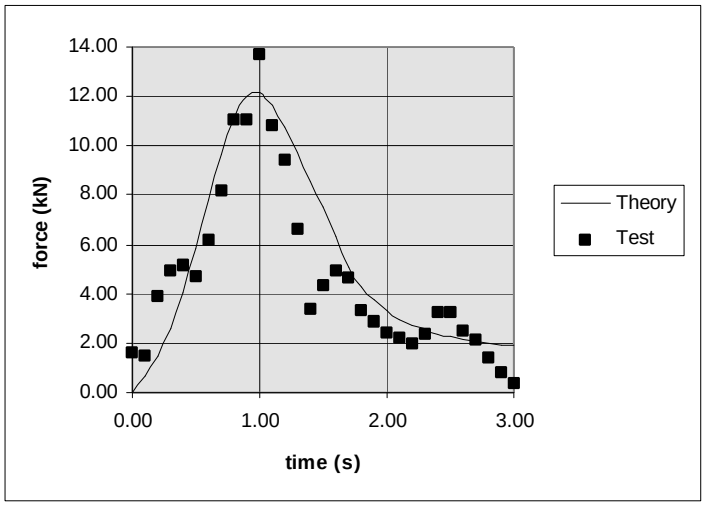

Figure 56 Simulation of the inflation load of a slider reefed ram-air parachute

The model was also used to simulate drop test 10 of the ARS from reference 9. The 334 m^2 is two stage reefed: 25.9% and 48.1% . The parachute and was dropped with a load of 6350 kg. The simulated data are shown in Figure 57. In the test the three inflation peaks were 47,000 lb, 38,000 lb and 27,000 lb. Again the match is satisfactory for a design calculation.

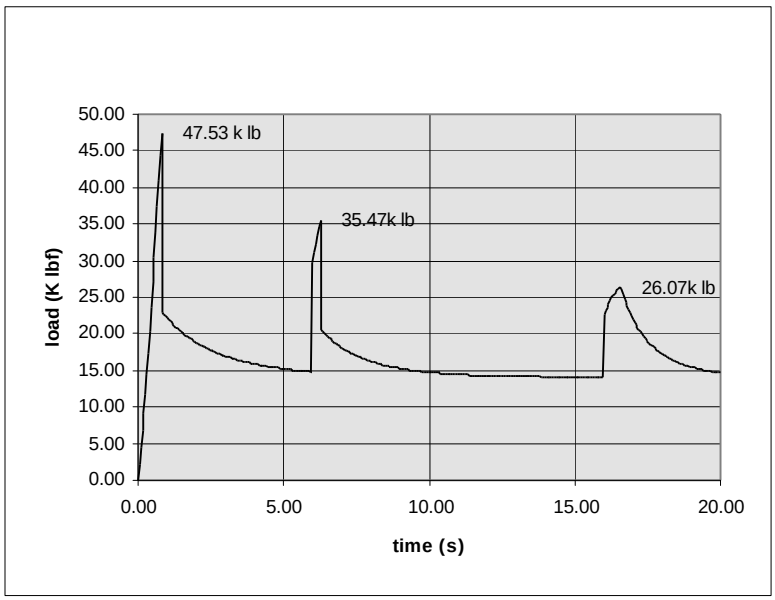

Figure 57 Simulation of the inflation load for a mid span reefed parachute, ARS drop test 10

In conclusion, whilst complete analysis of the inflation of ram-air parachutes is almost intractable engineering methods are available which give adequate predictions for design calculations.

REFERENCES

[1] W.K. Wailes — 'Advanced Recovery Systems for Advanced Launch Vehicles (ARS). Phase 1 Study Results.' AIAA-89-0881-CP (1989)

[2] Y. Li, H. Lin — 'Theoretical Investigation of Gliding Parachute Trajectory with Deadband Non-Proportional Automatic Homing Control.' AIAA-91-0834 (1989)

[3] J.S. Lingard — 'The Performance and Design of Ram-Air Gliding Parachutes.' RAE Technical Report TR 81103 (1981)

[4] T.F. Goodrick — 'Theoretical Study of the Longitudinal Stability of High Performance Gliding Airdrop Systems.' AIAA 75-1394 (1975)

[5] T.F. Goodrick — 'Simulation Studies of the Flight Dynamics of Gliding Parachute Systems.' AIAA 79-0417 (1979)

[6] J.S. Lingard — 'The Aerodynamics of Gliding Parachutes.' AIAA-86-2427-CP (1986)

[7] R.T. Mayer, E. Puskas, P. Lissaman — 'Controlled Terminal Descent and Recovery of Large Aerospace Components.' AIAA-86-2467-CP (1986)

[8] E. Puskas — 'The Development of a 10,000lb Capacity Ram-Air Parachute.' AIAA- 89-0904-CP (1989)

[9] W.K. Wailes — 'Development Testing of Large Ram Air Inflated Wings.' AIAA-93-1204 (1993)

[10] T.F. Goodrick — 'Scale Effects on Performance of Ram Air Wings.' AIAA 84-0783 (1984)

[11] T. Chatzikonstantinou — 'Numerical Analysis of Three-Dimensional Non Rigid Wings.' AIAA-89-0907-CP (1989)

[12] T. Chatzikonstantinou — 'Recent Advances in the Numerical Analysis of Ram Air Wings using the Three-Dimensional Simulation Code "PARA3D".' AIAA-93-1203 (1993)

[13] P.B.S. Lissaman, G.J. Brown — 'Apparent Mass Effects on Parafoil Dynamics.' AIAA-93-1236 (1993)

[14] G.J. Brown — 'Parafoil Steady Turn Response to Control Input.' AIAA-93-1241 (1993)

[15] M.A. Gonzalez — 'Prandtl Theory Applied to Paraglider Aerodynamics.' AIAA-93-1220 (1993)

[16] J.C. Ross — 'Computational Aerodynamics in the Design and Analysis of Ram -Air Inflated Wings.' AIAA-93-1228 (1993)

[17] A. Pope — 'Basic wing and aerofoil theory.' New York, McGraw-Hill. (1951)

[18] S.F. Hoerner, H.V. Borst — 'Fluid - Dynamic Lift.' Brick Town, N.J., L.A. Hoerner (1975)

[19] J.D. Nicolaides — 'Parafoil Wind Tunnel Tests.' USAF Flight Dynamics Laboratory, Ohio, AFFDL-TR-70-146 (1971)

[20] G.M. Ware, J.L. Hassell, Jr. — 'Wind-Tunnel Investigation of Ram-Air Inflated All Flexible Wings of Aspect Ratios 1.0 to 3.0.' NASA TM SX-1923 (1969)

[21] C.H. Zimmerman — 'Characteristics of Clark Y aerofoils at small aspect ratio.' NACA Report 431 (1932)

[22] R.J. Speelman, C.A. Babish, R.J. Berndt — 'Parafoil Steerable Parachute, Exploratory Development for Airdrop System Application.' USAF Flight Dynamics Laboratory, Ohio, AFFDL-TR-71-37 (1972)

[23] S.F. Hoerner — 'Fluid Dynamic Drag.' New York, S.F. Hoerner (1965)

[24] K-F. Doherr, C. Saliaris — 'Dynamic Stability Analysis of Parachutes' CCG-University of Minnesota, Parachute Systems Technology Short Course, Oberpfaffenhofen (June 1987)

[25] D.O. Dommasch, S.S. Sherby, T.F. Connolly — 'Airplane Aerodynamics.' Pitman Aeronautical Publications (1951)

[26] K-F. Doherr *et al* — 'Pre-Stuudy on Parachutes for a Crew Transport Vehicle - Capsule Recovery System Volume 3 Advanced Recovery System Concept.' DLR Technical Report HT-TN-E9-3-DLR (1994)

[27] T.W. Knacke — 'Parachute Recovery Systems Design Manual.', NWC TP 6575, Para Publishing, Santa Barbara, California. ISBN 0-915516-85-3 (1992)

[28] W.P Ludtke — 'A technique for Calculation of the Opening Shock Forces for Several Types of Solid Cloth Parachutes.', AIAA 73-477 (1973)

[29] J.S Lingard — 'A Semi-Empirical Theory to Predict the Load Time History of an Inflating Parachute.', RAE Technical Report 79141 (1979)

[30] R.J. McGhee, W.D. Beasley — 'Low Speed Aerodyanmci Characteristics of a 17-Percent Thick Airfoil Section Designed For General Aviation.', NASA TN D-7428 (1973)